AN ABSTRACT OF THE THESIS OF

Christopher H. Gifford-Miears for the degree of Master of Science in Civil Engineering presented on December 4, 2013.

Title: A Novel Framework for Uncertainty Propagation in River Systems based on Performance Graphs using Two-dimensional Hydrodynamic Modeling

Abstract approved: _____

Arturo S. Leon

This thesis presents a novel approach for propagation of uncertainty in river systems. Errors in data observations and predictions (e.g., stream inflows), in model parameters, and resulting from the discretization of continuous systems, all point to the need to accurately quantify the amount of uncertainty carried through the modeling process. In the proposed framework, stochastic processes are incorporated directly into the physical description of the system (e.g., river flow dynamics) with the goal of better modeling uncertainties (both aleatoric and epistemic) and hence, reducing the ranges of the confidence intervals on quantities of interest. We represent uncertainty in stream inflows via an error term modeled as a stochastic process. Stochastic collocation is then used to discretize random space. This non-intrusive approach is both more efficient than Monte-Carlo methods and is as flexible in its application. The flow dynamics are simulated efficiently using the performance graphs approach implemented in the OSU Rivers model. For one-dimensional unsteady flow routing, the performance graph (PG) approach has been shown to be accurate, numerically efficient, and robust. The Hydraulic Performance Graph (HPG) of a channel reach graphically summarizes the dynamic relation between the flow through and the stages at the ends of the reach under gradually varied flow (GVF) conditions, while the Volumetric Performance Graph (VPG) summarizes the corresponding storage. The hydraulic routing for the entire system consists of dividing the river system into reaches and pre-computing the hydraulics for each of

these reaches independently using a steady flow model. Then, a non-linear system of equations is solved that is assembled based on information summarized in the systems' performance graphs, the reach-wise equation of conservation of mass, continuity and water stage compatibility conditions at the union of reaches (nodes), and the system boundary conditions. For complex flows in river systems such as when there is flow over floodplains, the dynamic relation between water stages and flow in a river reach is best represented by depth averaged two-dimensional hydrodynamic models. The applicability of two-dimensional flow modeling for the construction of PGs for unsteady flow routing in complex river networks is explored. To illustrate application of the uncertainty propagation framework and PGs derived from two-dimensional flow models, a test case is presented that examines uncertainty quantification and flood routing through a complex section of the Fraser River in British Columbia.

A Novel Framework for Uncertainty Propagation in River Systems based on Performance Graphs using Two-dimensional Hydrodynamic Modeling

by

Christopher H. Gifford-Miears

A THESIS

submitted to

Oregon State University

in partial fulfillment of
the requirements for the
degree of

Master of Science

Presented December 4, 2013
Commencement June 2014

Master of Science thesis of Christopher H. Gifford-Miears presented on December 4, 2013.

APPROVED:

Major Professor, representing Civil Engineering

Head of the School of Civil and Construction Engineering

Dean of the Graduate School

I understand that my thesis will become part of the permanent collection of Oregon State University libraries. My signature below authorizes release of my thesis to any reader upon request.

Christopher H. Gifford-Miears, Author

ACKNOWLEDGEMENTS

I would like to express my gratitude to my advisor, Dr. Arturo S. Leon, for his support, guidance, and encouragement throughout my graduate studies. His technical advice was essential to the completion of this thesis and has taught me innumerable lessons in hydraulics and academic research in general.

I would also like to gratefully acknowledge the financial support of the Bonneville Power Administration (US Department of Energy) through the Contract TIP#258 *Development of a State-of-the-Art Computational Framework and Platform for the Optimal Control of Multi-Reservoir Systems Under Uncertainty.*

Thank you to Northwest Hydraulic Consultants (NHC) of Vancouver, B.C. for providing bathymetric and Acoustic Doppler Current Profiler (ADCP) data used for the hydrodynamics work performed in this thesis.

I would like to thank all of my family and friends for their support during my graduate studies. Through all of their encouragement, moral support, and edible support, I have been enabled to complete this goal. I am especially grateful to Sarah, for her love and understanding during the past couple of years. Her support, late-night calls, and writing criticisms were invaluable to the completion of this thesis.

Finally, I would also like to thank all of the professors and graduate students with whom I've had the pleasure of meeting and working with at Oregon State University.

CONTRIBUTION OF AUTHORS

Luis Gomez assisted in both updating and improving the OSU-Rivers Unsteady Routing model used for the final analysis of Chapter 2. Professor Nathan Gibson from the Oregon State University, Department of Mathematics, contributed with the overall writing and design of Chapter 3. Lastly, Post-doc Veronika Vasylkivska, Oregon State University, Department of Mathematics contributed the code used for discretization of the stochastic inflows via Karhuneń Loeve expansion.

TABLE OF CONTENTS

TABLE OF CONTENTS (Continued)

LIST OF FIGURES

LIST OF FIGURES (Continued)

Figure Page

LIST OF TABLES

LIST OF APPENDIX FIGURES

Chapter 1: Introduction

Uncertainties play a major role in the management of regulated river systems and if unaccounted for, can lead to hydropower revenue losses, flooding events, or general ineffective management of water resources. In the case of operational decisions in regulated river systems, (e.g. Columbia River Basin) strict socio-economic constraints require an understanding of modeling uncertainties (e.g. stream inflows) and how they propagate through the system. It is not sufficient to merely understand the magnitude of these uncertainties, but it is also necessary to be able to quantify the sensitivity of the system to the uncertainties in individual model parameters and forcings. In this thesis two components of a larger project are covered, namely efficient unsteady hydraulic routing and uncertainty propagation in river systems.

The Pacific Northwest has by far the largest fraction of hydropower use in the U.S. (around 70%), most of which is produced at thirty federally owned dams (Payne et al., 2004). These reservoirs serve many functions including flood protection, hydropower generation, and recreation. Bonneville Power Administration (BPA) is the Northwest's federal marketer for Columbia River hydroelectric power. The BPA real-time operations planning group makes operational decisions based on projections and forecasts for stream inflows and energy market pricing on an hourly to daily operational time frame. For short-term operational problems, stream inflows may be generated from forecasting models, in which case the primary source of uncertainty is the forecast error (Labadie, 2004). Based on uncertainty in the forecast inflows, it becomes necessary to quantify the uncertainty for operation metrics (e.g. discharge, water stage) in a robust and efficient manner. In chapter 3, a novel uncertainty quantification framework is proposed that correlates the response of the reservoir operation metrics to the uncertainty in the forecast inflows, through dynamics of the river flow.

Open-channel flows in natural river systems are generally unsteady and non-uniform. Spatial and temporal changes in flow discharge and water stages derive from precipitation run-off, snow melt, reservoir operations in regulated river systems as well as many other sources. Modeling of unsteady river hydraulics is achieved through discretizing and

solving the conservation of mass and momentum equations. The Saint-Venant equations, or dynamic-wave model, are one such pair of partial differential equations. No exact analytic solution exists for the Saint-Venant equations (except for special cases) and the developed numerical schemes must adhere to strict spatial and temporal criterion to attain stability. However, despite the developed numerical schemes, robustness is still a problem (González-Castro, 2000). For one-dimensional unsteady flow routing, the performance graph (PG) approach has been shown to be accurate, numerically efficient, and robust (Leon et al., 2013a). Chapter 2 in this thesis expands upon previous PG work to utilize two-dimensional depth-averaged hydrodynamic simulations in the construction of PGs for unsteady flow routing.

This thesis is presented in two major parts. The first part explores unsteady flow routing utilizing performance graphs generated from two-dimensional hydrodynamic simulations and the second presents an uncertainty propagation framework for use in river systems. The performance graph unsteady flow routing approach is used to represent the river flow dynamics within the proposed uncertainty propagation framework. An application of the proposed framework is illustrated through a test case that examines uncertainty propagation and flood routing through a complex stretch of the Fraser River in British Columbia.

Chapter 2: Unsteady flow routing using Performance Graphs based on two-dimensional hydrodynamic simulations

2.1 Introduction

When considering optimization problems that involve river systems, hundreds or thousands of simulations may be required for each operational decision (e.g., gate operations). Depending on the operational time-scale, relevant hydraulic information throughout the system may be required at a time resolution of an hour, or less (i.e. short-term operation) (Fleten and Kristoffersen, 2008). Hence, robust and numerically efficient hydraulic routing methods are necessary.

A standard method for modeling unsteady flows in rivers is the application of the Saint-Venant equations. The Saint-Venant equations are a set of non-linear, partial differential equations that describe one-dimensional, unsteady open-channel flow. The Saint-Venant equations consist of conservation of mass and momentum equations and can be written as Equations (2.1) and (2.2), respectively (Leon et al., 2013a):

$$\frac{\partial A}{\partial t} + \frac{\partial Q}{\partial x} = 0 \tag{2.1}$$

$$\frac{1}{g}\frac{\partial V}{\partial t} + \frac{\partial}{\partial x}\left(\frac{V^2}{2g}\right) + cos\theta\frac{\partial h}{\partial x} + S_f - S_o = 0 \tag{2.2}$$

where x = the distance along the channel; t = time, V = cross-sectional velocity; g = acceleration due to gravity; h = flow depth normal to x; A = cross-sectional area; Q = discharge; θ = angle between the channel bed and horizontal plane; S_o = bed slope; S_f = friction slope. The five terms in momentum equation, Eq. (2.2), [from left to right] represent the local and convective acceleration, pressure force, friction force, and gravity force respectively.

Due to non-linear terms in the Saint-Venant equations (i.e. convective acceleration), no exact analytic solution exists, except for special cases. Numerical methods used to solve the one-dimensional Saint-Venant equations include the Method of Characteristics, finite-difference, finite-element, and finite-volume schemes (Cunge et al. (1980) and Chaudhry (2008)). Classic methods for solving the Saint-Venant equations are also presented in (Mahmood et al., 1975), (Abbott, 1979), (Cunge et al., 1980), (Chaudhry, 2008), and others. Despite the wide array of numerical methods available for solving the Saint-Venant equations, the lack of robustness (e.g., instabilities) and accuracy issues still poses a problem (Leon et al., 2013a).

In an effort to address the issue of robustness and accuracy when solving the Saint-Venant equations, there have been several studies and applications determining suitability of simplified versions of the full Saint-Venant equations, or also called the dynamic wave equation (e.g., Henderson, 1966; Tsai, 2003). Common approximations of the dynamic wave equation for use in unsteady flow routing include quasi-steady dynamic wave, noninertia wave, and kinematic wave models. Each of the aforementioned models exclude physical terms of the momentum equation, Eq. (2.2), to reduce computational complexity. The quasi-steady dynamic wave approximation for example, includes all terms in the full dynamic wave equation, Eq. (2.2), except for the local acceleration (i.e. $\frac{\partial V}{\partial t}$). Details for selection criteria to determine applicability of each approximation to unsteady flow routing can be found in (Ponce et al., 1978; Tsai, 2003).

A relatively new method for hydraulic routing of unsteady, open-channel flows utilizes Hydraulic performance graph (HPG) theory (Yen and González-Castro, 2000; González-Castro, 2000). HPGs summarize the dynamic relationship between the water depths, or stages, at the upstream and downstream ends of a channel reach for a range of specified discharges. This family of channel delivery curves, or hydraulic performance curves (HPCs) (Bakhmeteff, 1932), stores precomputed solutions to the gradually varied flow (GVF) profiles for each reach, through all possible operating conditions. The theory of HPGs was further improved by Ben Chie Yen's research group at the University of Illinois at Urbana-Champaign. HPGs have since been applied to various open channel hydraulic studies such as:

1. hydraulic performance of floodplain channels under pre- and post-breached levee conditions (González and Yen, 1996)

2. carrying capacity assessment of channel systems in series (Yen and González-Castro, 2000)

3. applicability of Hydraulic Performance Graphs to unsteady flow routing in channels and channels in series (González-Castro, 2000)

4. theoretical development of discharge ratings based on the hydrodynamics of unsteady and nonuniform flows (Schmidt, 2002)

5. unsteady flow routing in sewers maintaining mass conservation by pre-computing

the reach volume for each HPG flow condition, and storing as Volumetric Performance Graphs (VPGs) (Hoy and Schmidt, 2006a)

6. flood control coupling HPG/VPG unsteady flow routing and NSGA-II optimization (Leon et al., 2013b)

7. unsteady flow routing in looped and dendritic open-channel networks (Leon et al., 2013a)

8. pressurized and supercritical flows in a combined sewer system optimization model (Zimmer et al., 2013)

Unsteady open-channel flow routing is achieved in this paper utilizing the performance graph (PG) approach applied to dendritic and looped networks as presented in (Leon et al., 2013a). HPGs summarize the discharge capacity of an open channel as a function of the downstream water surface elevation (Yen and González-Castro, 2000), and accounts for the conservation of momentum, Eq. (2.2). VPGs summarize the corresponding channel reach volume for each HPG flow scenario, accounting for conservation of mass, Eq. (2.1). HPGs and VPGs are then accessed as look-up tables rather than performing repetitive backwater calculations, and can be used to simulate unsteady flows through dendritic and looped networks. Given that the hydraulics of each reach are precomputed, the PG approach results in a robust and computationally efficient tool for analyzing unsteady river flows.

Even though HPGs were used in a wide array of applications, the use of two-dimensional (2D) hydrodynamic models for the construction of PGs for unsteady flow routing has not yet been investigated. In a river system with complex flow features, a two-dimensional model is better suited to capture and represent two-dimensional flow structures (e.g. horizontal eddies). This paper explores the use of a depth averaged two-dimensional (2D) hydrodynamic model for the construction of PGs and their application to unsteady flow routing. The model utilized for PG unsteady flow routing is OSU-Rivers, the Oregon State University unsteady routing model (Leon et al., 2013a). The two-dimensional performance graphs (2D-PGs) are later applied to a test section of the Fraser River in British Columbia.

2.2 Hydraulic Performance Graphs

The following describes the basic procedure required to create a HPG, adapted from (González-Castro and Yen, 2000).

1. Divide the river system into reaches, making sure that the flow is near one-dimensional at the ends of each reach.
2. Determine the ranges of water depth, or water stages, to be considered at the reach ends.
3. Determine and plot the Z-line which is composed of water surface elevation pairs representing a horizontal water level (i.e. $WSE_{ds} = WSE_{us}$). Where $WSE =$ water surface elevation and subscripts ds and us refer to downstream and upstream ends of a reach respectively.
4. For mild-sloped channels with M1- or M2- type backwater profiles:
   (a) Select a constant discharge value (Q)
   (b) Set the downstream boundary condition to a fixed water stage, WSE_{ds}
   (c) Compute the backwater profile using a gradually varied flow (GVF) model to obtain upstream water stage, WSE_{us}
   (d) Store resulting upstream water stage value, where $WSE_{us} = f(WSE_{ds}, Q)$
5. Repeat steps 1 through 3 until adequate resolution is achieved

For further details about the HPG and VPG generation the reader is referred to (González-Castro, 2000), (Hoy and Schmidt, 2006a) and (Leon et al., 2013a).

2.3 Governing Equations

The open source TELEMAC-2D (Galland et al., 1991; Hervouet, 2007) model was used to build the 2D-PGs. TELEMAC-2D uses finite-element and finite-volume methods to solve the two-dimensional depth-averaged free surface flow equations (also known as the shallow water or 2D Saint-Venant equations) in non-conservative depth-velocity form (Hervouet, 2007). Finite-element methods are used in this study. TELEMAC-2D solves the following equations:

Continuity Equation:

$$\frac{\partial h}{\partial t} + \frac{\partial (hV_x)}{\partial x} + \frac{\partial (hV_y)}{\partial y} = 0 \tag{2.3}$$

x-momentum direction:

$$\frac{\partial V_x}{\partial t} + V_x \frac{\partial V_x}{\partial x} + V_y \frac{\partial V_x}{\partial y} = -g \frac{\partial Z_s}{\partial x} + F_x + \frac{1}{h} \bigtriangledown \cdot [h \nu_T \overrightarrow{\bigtriangledown} (V_x)] \tag{2.4}$$

y-momentum direction:

$$\frac{\partial V_y}{\partial t} + V_x \frac{\partial V_y}{\partial x} + V_y \frac{\partial V_y}{\partial y} = -g \frac{\partial Z_s}{\partial y} + F_y + \frac{1}{h} \bigtriangledown \cdot [h \nu_T \overrightarrow{\bigtriangledown} (V_y)] \tag{2.5}$$

The F_x and F_y source terms represent the force induced by boundary friction, where the depth averaged volume force in terms of Manning coefficient, n, is given by:
x-direction:

$$F_x = -\frac{1}{cos\theta} \frac{gn^2}{h^{4/3}} V_x \sqrt{V_x^2 + V_y^2} \tag{2.6}$$

y-direction:

$$F_y = -\frac{1}{cos\theta} \frac{gn^2}{h^{4/3}} V_y \sqrt{V_x^2 + V_y^2} \tag{2.7}$$

Where t = time; x and y = horizontal Cartesian coordinates; h = flow depth; V_x and V_y = depth-averaged flow velocities in x and y directions respectively; Z_s = water surface elevation; g = gravitational acceleration; θ = angle between the channel bed and longitudinal plane; ν_T = turbulent viscosity.

Various turbulence closure schemes are implemented in TELEMAC-2D. An extended $k - \epsilon$ turbulence model is used herein. Due to the non-uniform vertical velocity profile, dispersion terms result when depth-integrating the Reynold's averaged Navier-Stokes equations (Hervouet, 2007). TELEMAC-2D employs an extension to the classical $k - \epsilon$ model that addresses these dispersion terms through source/sink terms in the transport equations (Rastogi and Rodi, 1978; Rodi, 1993). The $k - \epsilon$ model describes the turbulent viscosity as a function of the turbulent kinetic energy (k) and rate of dissipation (ϵ):

$$\nu_T = c_\mu \frac{k^2}{\epsilon} \tag{2.8}$$

where c_μ is an emperically derived constant typically equal to 0.09 (Launder and Spald-

ing, 1974). Transport of the turbulent kinetic energy and its dissipation are expressed as (Hervouet, 2007):

$$\frac{\partial k}{\partial t} + V_i \frac{\partial k}{x_i} = \frac{1}{h} \bigtriangledown \left(h \frac{\nu_T}{\sigma_k} \overrightarrow{\bigtriangledown}(k) \right) + P - \epsilon + P_{kv} \tag{2.9}$$

$$\frac{\partial \epsilon}{\partial t} + V_i \frac{\partial \epsilon}{x_i} = \frac{1}{h} \bigtriangledown \left(h \frac{\nu_T}{\sigma_\epsilon} \overrightarrow{\bigtriangledown}(k) \right) + \frac{\epsilon}{k} \left(C_{1\epsilon} P - C_{2\epsilon} \epsilon \right) + P_{\epsilon v} \tag{2.10}$$

where turbulent kinetic energy production, P, is calculated by horizontal velocity gradients shown in tensorial form (e.g. indices i and j = 1,2):

$$P = \nu_T \left(\frac{\partial V_i}{\partial x_j} + \frac{\partial V_j}{\partial x_i} \right) \frac{\partial V_i}{\partial x_j} \tag{2.11}$$

P_{kv} and $P_{\epsilon v}$ are source terms due to shear force of flow along the vertical plane:

$$P_{kv} = C_k \frac{{V_*}^3}{h} \text{ and } P_{\epsilon v} = C_\epsilon \frac{{V_*}^4}{h^2}$$

In these formulae:

$$C_k = \frac{1}{\sqrt{C_f}} \text{ and } C_\epsilon = 3.6 \frac{C_{2\epsilon} \sqrt{C_\mu}}{C_f^{\frac{3}{4}}}$$

where C_f = dimensionless friction coefficient (in our case, Manning's n); V_* = shear velocity (or friction velocity) and σ_k, σ_ϵ, $C_{1\epsilon}$, $C_{2\epsilon}$ represent closure coefficients for the standard $k - \epsilon$ model; the closure coefficients are typically assumed to take values of 1.0, 1.3, 1.44, and 1.92, respectively (Launder and Spalding, 1974). C_ϵ and C_k are determined on the basis of normal flow in the center of a rectilinear fluvial channel (Hervouet, 2007).

$$C_f = g n^2 / h^{1/3}$$

2.4 Suitability of two-dimensional hydrodynamics models for the construction of PGs

It is recalled that the PG approach is based on the one-dimensional steady gradually varied flow approximation of the Saint-Venant equation (González-Castro, 2000). This

is equivalent to the so-called quasi-steady dynamic wave approximation which for a near horizontal channel is given by (e.g., González-Castro, 2000)

$$\frac{V}{g}\frac{\partial V}{\partial x}+\frac{\partial h}{\partial x}-(S_o-S_f)=0, \tag{2.12}$$

Since the flow is steady, V and h are a function of x only and hence the partial derivatives in Equation (2.12) can be replaced with total derivatives. The resulting equation can be discretized as

$$\frac{1}{2g}\frac{\Delta V^2}{\Delta x}+\frac{\Delta h}{\Delta x}-\left(-\frac{\Delta z}{\Delta x}-\frac{h_f}{\Delta x}\right)=0, \tag{2.13}$$

By eliminating Δx in Equation (2.13) and applying this equation between two consecutive sections 1 and 2 (1 is upstream of 2) gives

$$h_1+\frac{U_1^2}{2g}+z_1=h_2+\frac{U_2^2}{2g}+z_2+h_f \tag{2.14}$$

The energy equation in integral form for a control volume CV bounded by a control surface CS can be written as (e.g., Kleinstreuer, 1997)

$$\dot{Q}+\dot{W}_{shear}=\frac{\partial}{\partial t}\int\left(u+\frac{\left|\vec{U}^2\right|}{2}+gz\right)\rho dV+\int_{cs}\left(u+\frac{p}{\rho}+\frac{\left|\vec{U}^2\right|}{2}+gz\right)\rho\vec{U}\cdot\vec{n}dA, \tag{2.15}$$

where u is the internal energy, $\vec{U}^2/2$ is the kinetic energy and gz is the potential energy, p is pressure, ρ is density, g is the acceleration of gravity, A is area, n is the unit normal vector to the control surface, $\dot{Q}$ is the rate of heat added on system, $\dot{W}_{shear}$ is the shear work done on system. For a steady flow the first term of the right hand side is zero. In addition, for uniform flow properties at the inlet (section 1) and outlet (section 2) [see Figure 2.1] with control sections normal to the local flow direction, Equation (2.15) can be reduced to (e.g., Kleinstreuer, 1997):

$$\frac{p_1}{\rho_1}+\frac{\left|\vec{U}_1^2\right|}{2}+gz_1=\frac{p_2}{\rho_2}+\frac{\left|\vec{U}_2^2\right|}{2}+gz_2+\left[u_2-u_1-\frac{\dot{Q}}{\dot{m}}-\frac{\dot{W}_{shear}}{\dot{m}}\right] \tag{2.16}$$

where $\dot{m}$ is the mass flow rate. The term in square brackets in Equation (2.16) is the

total head loss and hence, this equation can be written as (e.g., Kleinstreuer, 1997)

$$h_1 + \frac{U_1^2}{2g} + z_1 = h_2 + \frac{U_2^2}{2g} + z_2 + h_{loss} \tag{2.17}$$

which is the typical representation of the energy equation. Note in Equation (2.16) that uniform flow properties need to be insured only at the inlet and outlet of the control section. The reader can notice that Equations (2.14) and (2.17) are the same and hence it is expected that one and higher-order gradually varied flow models are suitable for constructing PGs.

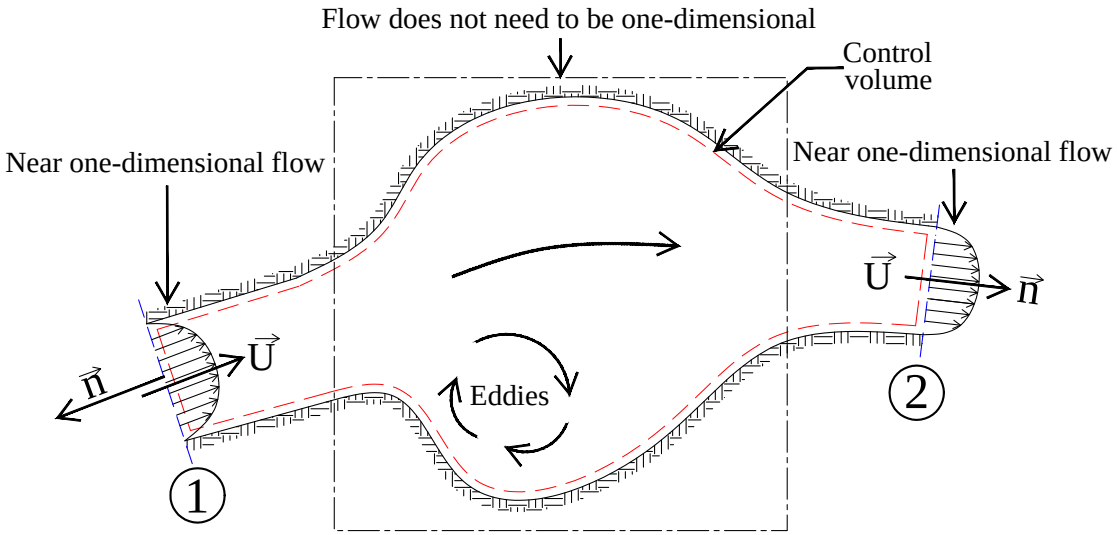

Figure 2.1: Control volume representation within a 2D-PG reach; $\vec{n}$ and $\vec{U}$ represent the outward normal and velocity vectors, respectively

2.5 Fraser River Application

For demonstration purposes, the OSU-Rivers model, using 2D-PGs, is applied to the Fraser River near Vancouver, British Columbia. By volume, the Fraser River is the largest river in British Columbia and the fifth largest in Canada. Fraser River is also the tenth longest river in Canada, flowing with a length of 1,375 kilometers. The Fraser River test section extends from 500 meters downstream of the Patullo Bridge in Vancouver,

Canada, to approximately 6.5 kilometers upstream. As shown in Fig. (2.2), the river reach consists of a branching flow around an island with a guiding dike upstream of the island. Because of the complex bathymetry of the river around the island, and it's associated flow, two-dimensional PGs will be used to summarize the hydraulics and corresponding head-losses.

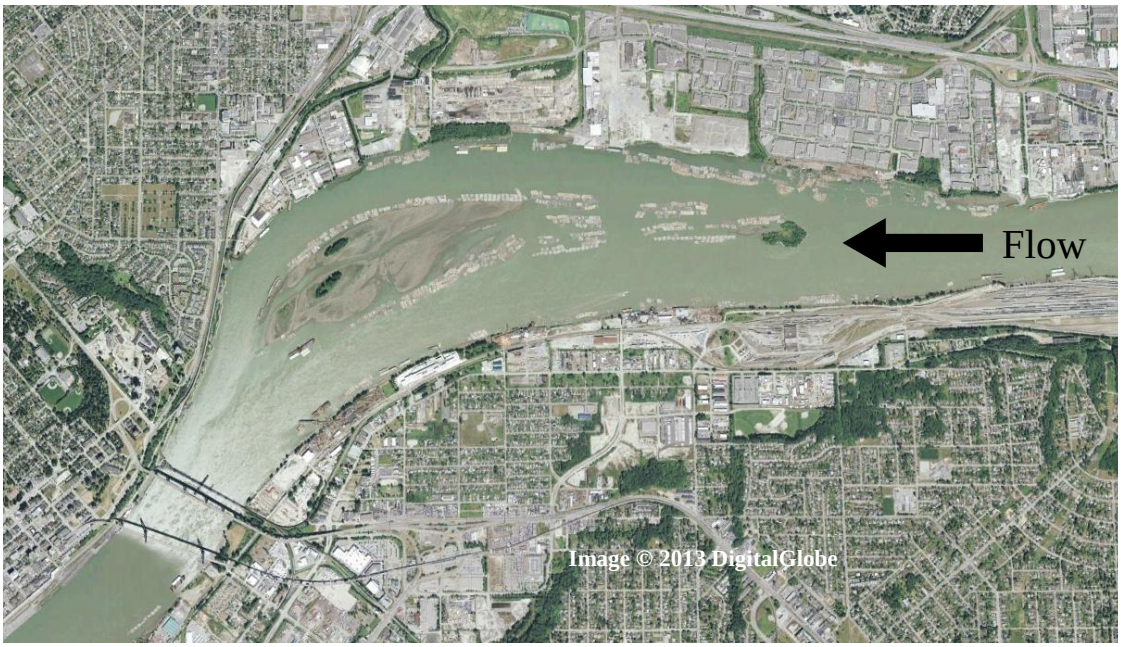

Figure 2.2: Fraser River test case: 6.5 Kilometer river section neighboring New Westminster, British Columbia (flow is from right to left)

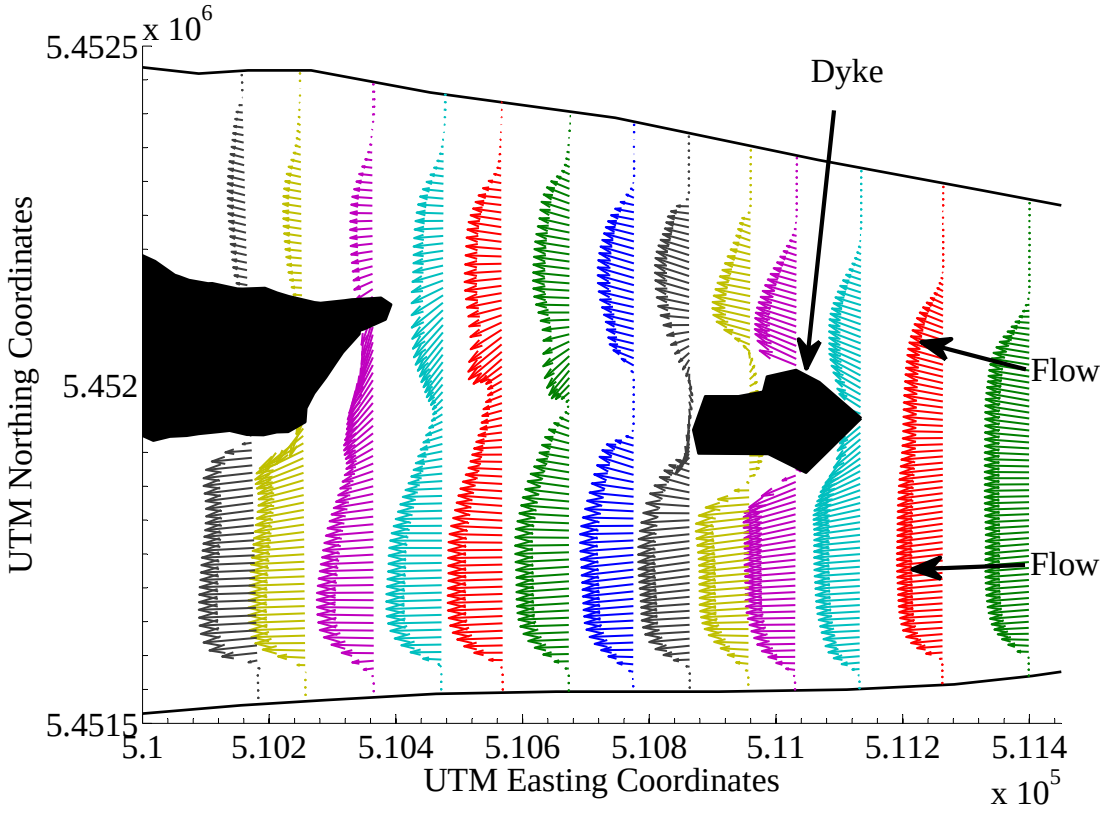

Figure 2.3: Plan view of velocity flow field downstream of flow guiding dyke

Table 2.1: Reach characteristics of Fraser River test case

Reach ID	Upstream section	Downstream section	Length (m)	z_u (m)	z_d (m)
US-1	1	2	288.05	10.00	10.97
US-2	2	3	434.78	10.97	13.28
US-3	3	4	609.93	13.28	14.97
RB-0	4	5	274.33	14.97	13.99
RB-1	5	6	1582.08	13.99	20.08
RB-2	6	7	344.78	20.08	19.75
RB-3	7	8	478.21	19.75	16.65
RB-4	8	9	460.28	16.65	17.99
RB-5	9	10	343.74	17.99	17.73
RB-6	10	11	275.74	17.73	16.12
RB-7	11	12	304.40	16.12	16.00
RB-8	12	13	337.92	16.12	12.01
RB-9	13	14	137.24	12.01	9.77
LB-0	4	15	305.90	14.97	12.18
LB-1	15	16	1489.62	12.18	14.19
LB-2	16	17	506.62	14.16	12.03
LB-3	17	18	500.67	12.09	11.73
LB-4	18	19	562.02	11.73	13.81
LB-5	19	20	330.46	13.81	12.30
LB-6	20	14	156.72	12.30	9.77
DS-4	14	21	688.43	9.77	4.60
DS-5	21	22	570.00	4.60	12.30

2.5.1 Grid Generation

As illustrated in the previous section, the PG assumption requires that the flow is near one-dimensional (e.g., no recirculation) at the upstream and downstream ends of a reach (e.g. Figure 2.4). The flows inside the reach do not need to be one-dimensional. For this study, the Fraser River stretch was divided into eighteen reaches as shown in Figure

(2.5). Fraser River PG reach characteristics are shown in Table 2.1. An unstructured, triangular element mesh was generated to represent both the Fraser River domain mesh as well as the 18 individual PG reaches. Each mesh was generated by constrained Delaunay Triangulation using the freely available meshing tool, Blue Kenue, developed by the Canadian Hydraulics Centre of the National Research Council.

Spatial discretization of a river for the Performance Graph approach is dependent on bathymetric features and velocity profiles observed. Each reach is chosen so that the velocity profile at both the upstream and downstream ends are approximately one-dimensional (e.g. Fig. 2.4).

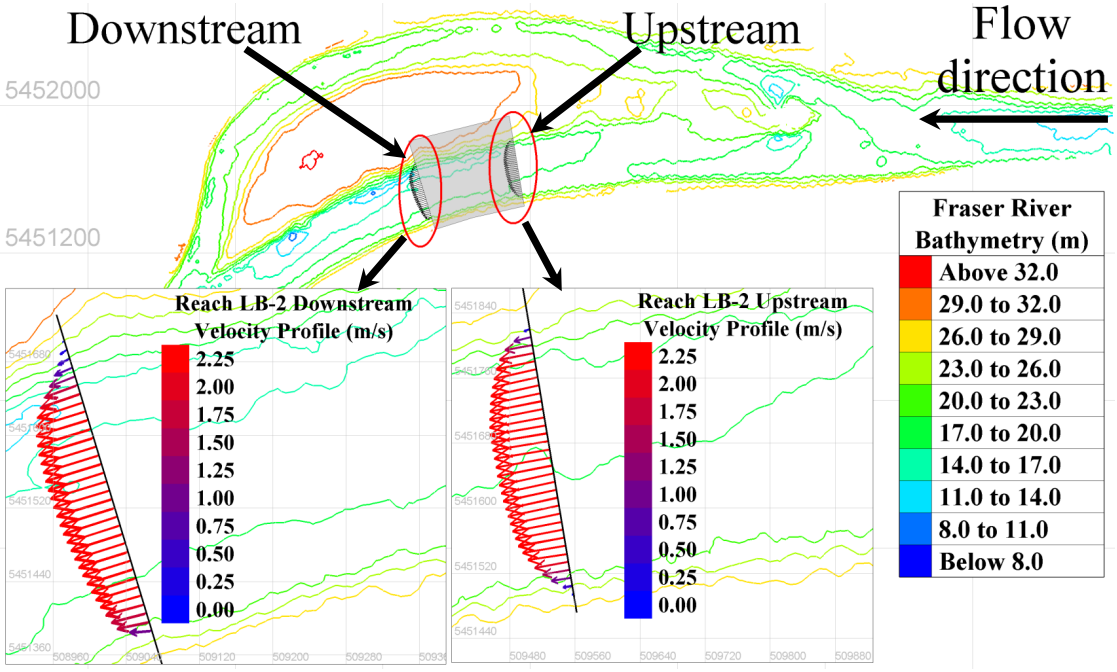

Figure 2.4: Example of approximately one-dimensional flow at the ends of reach LB-2

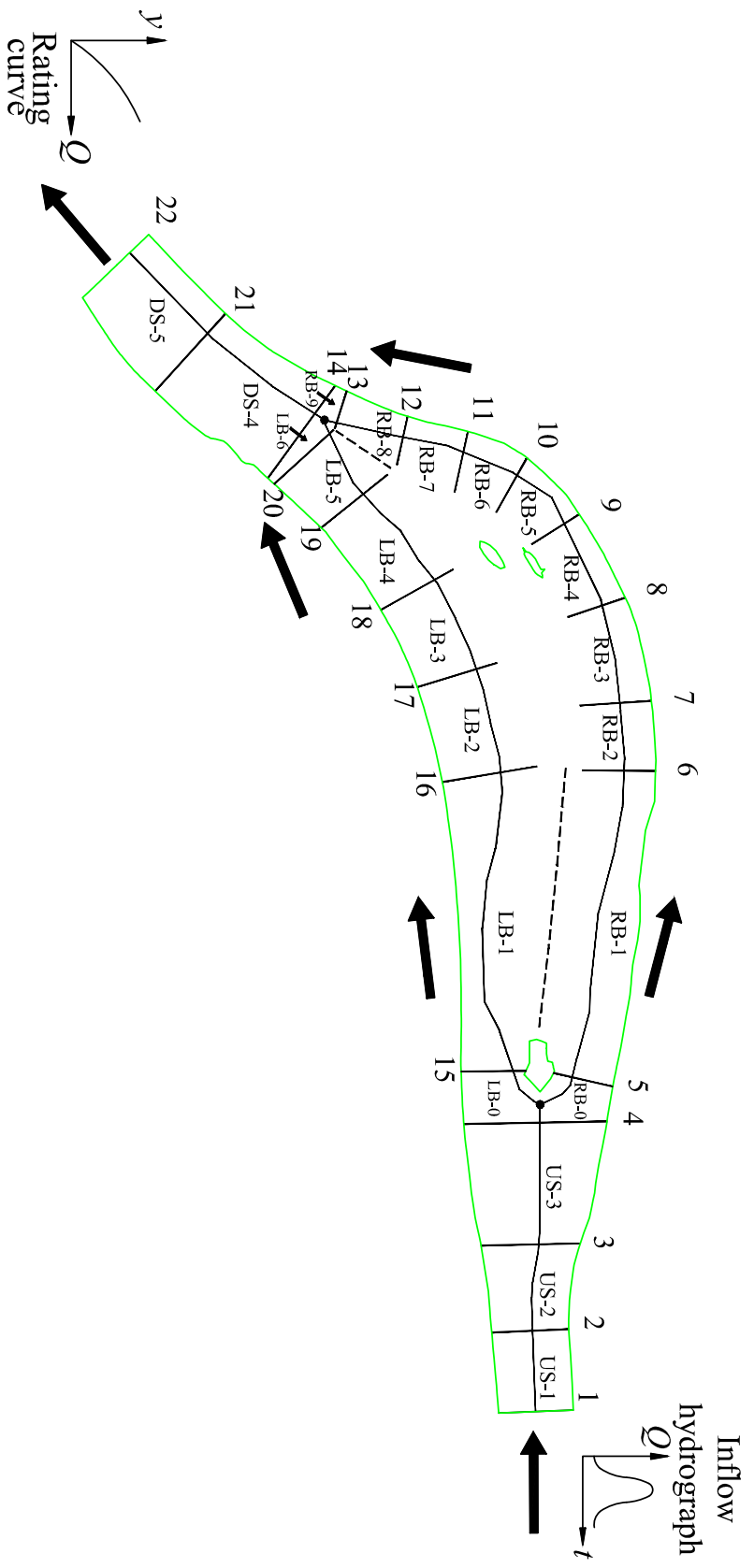

Figure 2.5: Test case of Fraser River divided into reaches for Performance Graph application

2.5.2 Boundary Conditions

The upstream boundary condition was an open boundary with specified discharge, while the downstream was an open boundary with specified water depth. Velocity distributions were assumed to have a velocity magnitude proportional to the square root of the depth at each upstream boundary node (i.e. $V \propto \sqrt{h}$).

In an effort to minimize the effect of the upstream discharge boundary condition, the mesh domain of each PG reach was extended as illustrated in Fig. (2.6). The purpose of extending the computational domain is to allow for flow development at the location of interest, which is the upstream end of the original reach.

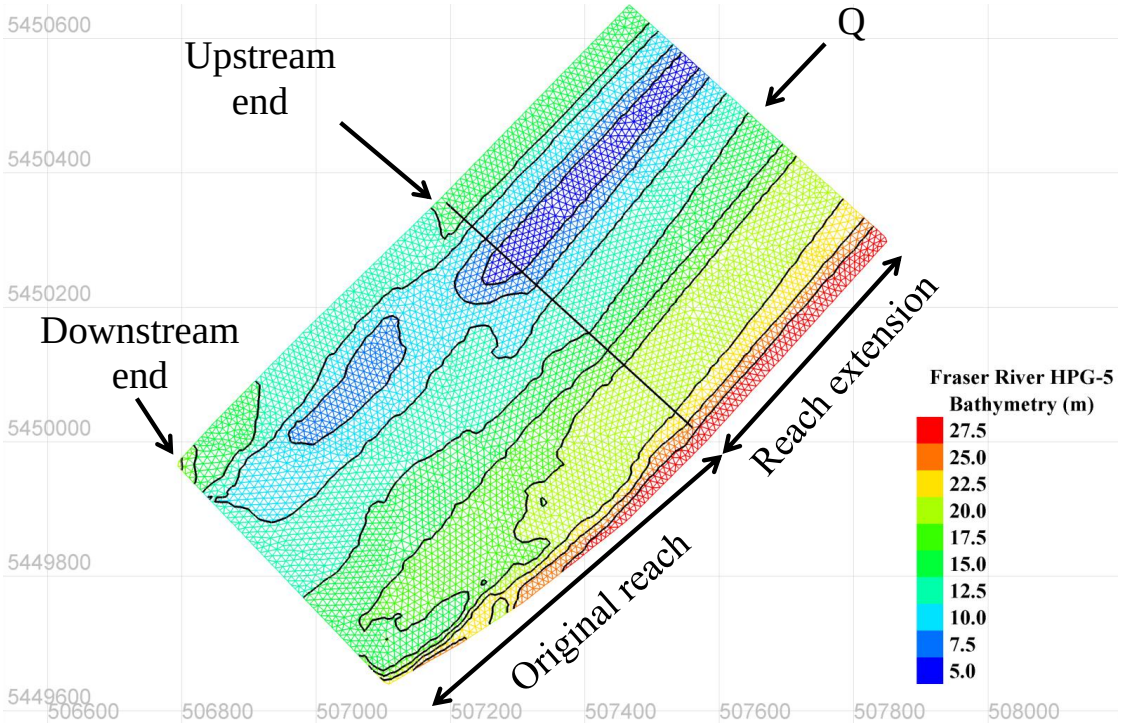

Figure 2.6: Extended reach at the upstream end to allow for flow development

2.5.3 Model Calibration

Calibration of the TELEMAC-2D model was performed using ADCP transect data provided by Northwest Hydraulic Consultants (NHC) of Vancouver, British Columbia. Simulated and measured velocity profiles for various transects are presented in Figures (2.8) and (2.9). The location of each ADCP transect measurement is shown in Figure (2.7). Through this comparison of measured and simulated velocities, a Mannings n value of 0.04 $m^{1/3}$ was utilized for the computational domain.

The Grid Convergence Index (GCI) (Celik et al., 2008) method was used to estimate the discretization error for the numerical study and provide an objective means for determining grid independence. The GCI is an index of the uncertainty associated with a solution at a particular grid resolution, in comparison to another grid resolution, based on the Richardson extrapolation (RE) theory (Hardy et al., 2003). Application of Richardson extrapolation theory as a component of the GCI requires that the flow field be sufficiently smooth for the quantity of interest, convergence is monotonic, and that the numerical method is in it's asymptotic range (Versteeg, 2007). The GCI procedure consists of five steps that systematically compare discrete solutions of a variable of interest, ϕ, between three or more grid resolutions, and estimate the discretization error multiplied by a factor of safety. A GCI value of zero would indicate that an exact solution has been achieved, which is not likely due to numerical and discretization errors. The Grid Convergence Index is calculated using the following equation:

$$GCI^{21}_{fine} = 1.25\frac{e^{21}_a}{r^p_{21} - 1} \tag{2.18}$$

Where superscripts 1 and 2 represent the fine and coarse mesh resolution, e_a = relative error between solutions 1 and 2, and r_{21} = ratio of representative element sizes, and p = apparent order of accuracy. Using a factor of safety of 1.25 is akin to providing a 95% confidence interval for solutions of interest (Hardy et al., 2003). Grid resolutions tested were $5m$, $10m$, and $20m$ element edge lengths using timesteps of 0.25, 0.50, and 1.00 second, respectively. Timestep sizes were chosen to maintain an approximately constant Courant number for each simulation. Grid resolutions and GCI values for variables of interest, water surface elevation (WSE) and discharge (Q), are shown in Tables 2.2 and 2.3, respectively.

According to Table 2.3, the numerical uncertainty on parameters of interest range from 0.1% to 1.51% on the finer grid (5m) and 0.46% to 2.78% on the coarser grid (10m). After comparing results for mesh element sizes of $5m$, $10m$, and $20m$, it was determined that $10m$ grid resolution was sufficient based on computational expense (e.g. each performance graph requires hundreds or thousands of simulations) and acceptable error for generation of performance graphs (e.g. Figs. 2.10 and 2.11).

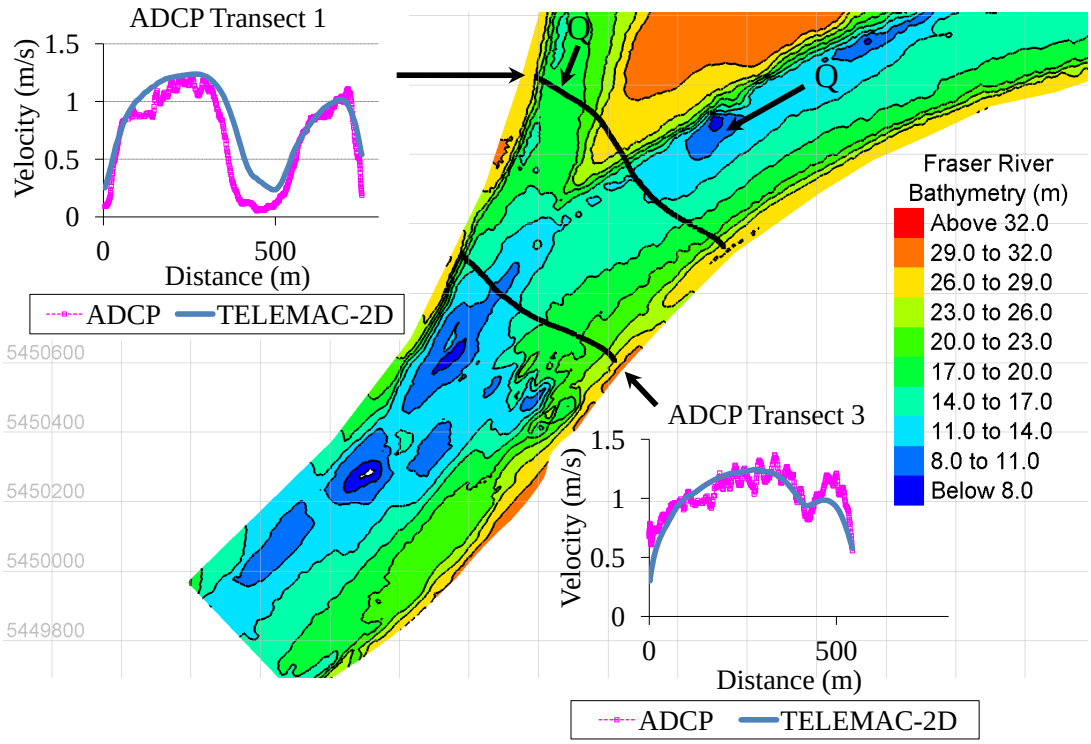

Figure 2.7: ADCP velocity transect measurements compared with results of TELEMAC-2D

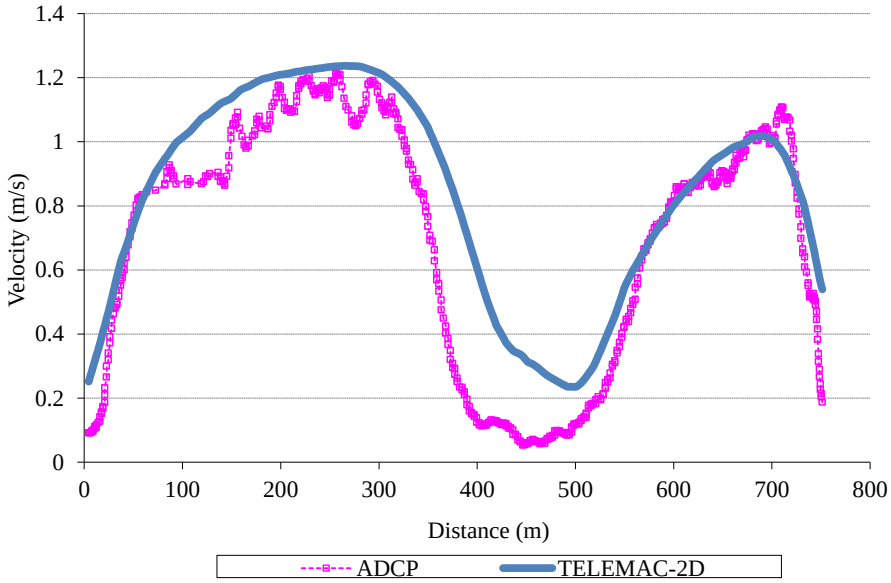

Figure 2.8: Transect 1 TELEMAC-2D versus ADCP velocity transect measurements

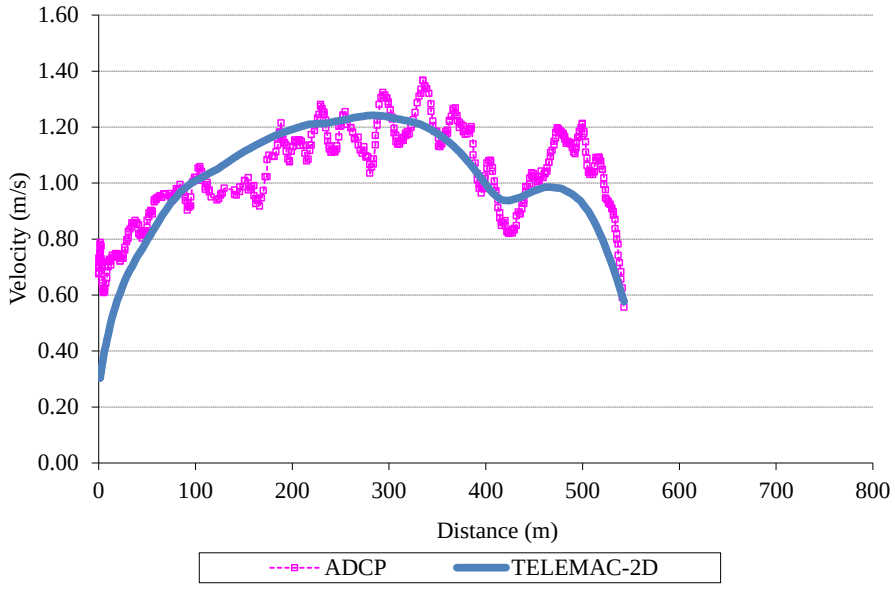

Figure 2.9: Transect 3 TELEMAC-2D versus ADCP velocity transect measurements

Table 2.2: Mesh used in the GCI analysis

Mesh	Element size (m)	Δt (s)	Number of elements N
1	5	0.25	456962
2	10	0.50	114218
3	20	1.00	28379

Table 2.3: Grid Convergence Index results

Reach	Location (See Figure 2.5)	Variable	$GCI^{21}_{fine(5m)}$ (%)	$GCI^{32}_{coarse(10m)}$ (%)
Upstream	Section 4	Average WSE	1.512	2.781
		Discharge, Q	0.011	0.035
Right branch	Section 8	Average WSE	0.387	1.049
		Discharge, Q	1.174	2.152
Left branch	Section 15	Average WSE	0.071	0.460
		Discharge, Q	0.553	0.667

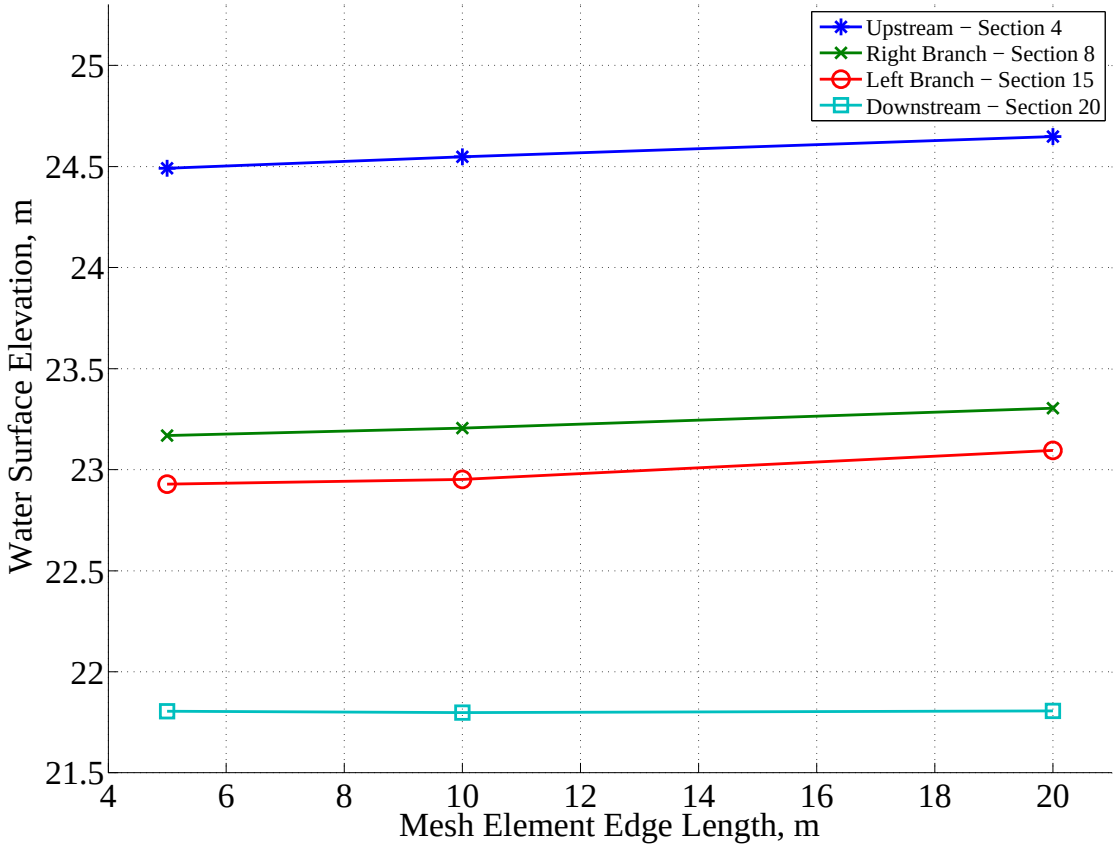

Figure 2.10: Water surface elevation mesh convergence results at multiple locations within the domain

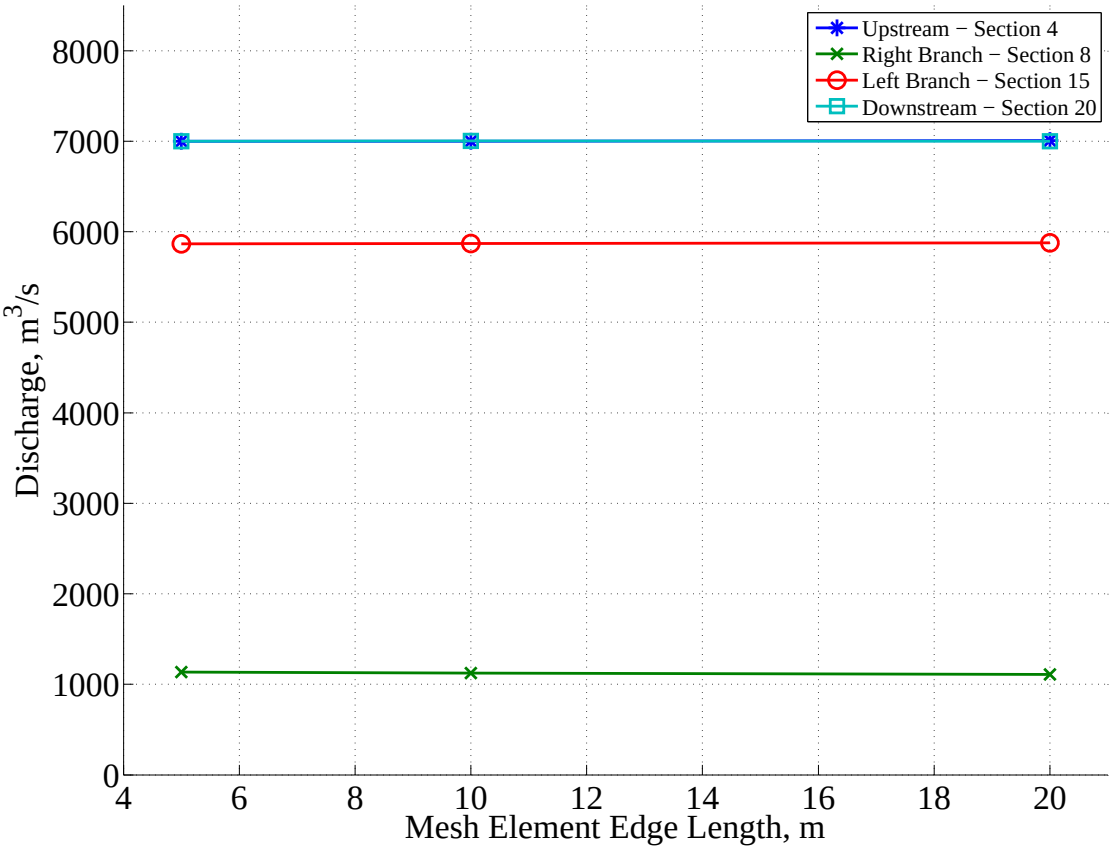

Figure 2.11: Discharge mesh convergence results at multiple locations within the domain

A major benefit of the performance graph approach is the ability to remove instabilities that could occur during the construction of the performance graphs. Figure (2.12) shows an example of an instability that was removed and re-simulated with updated parameters.

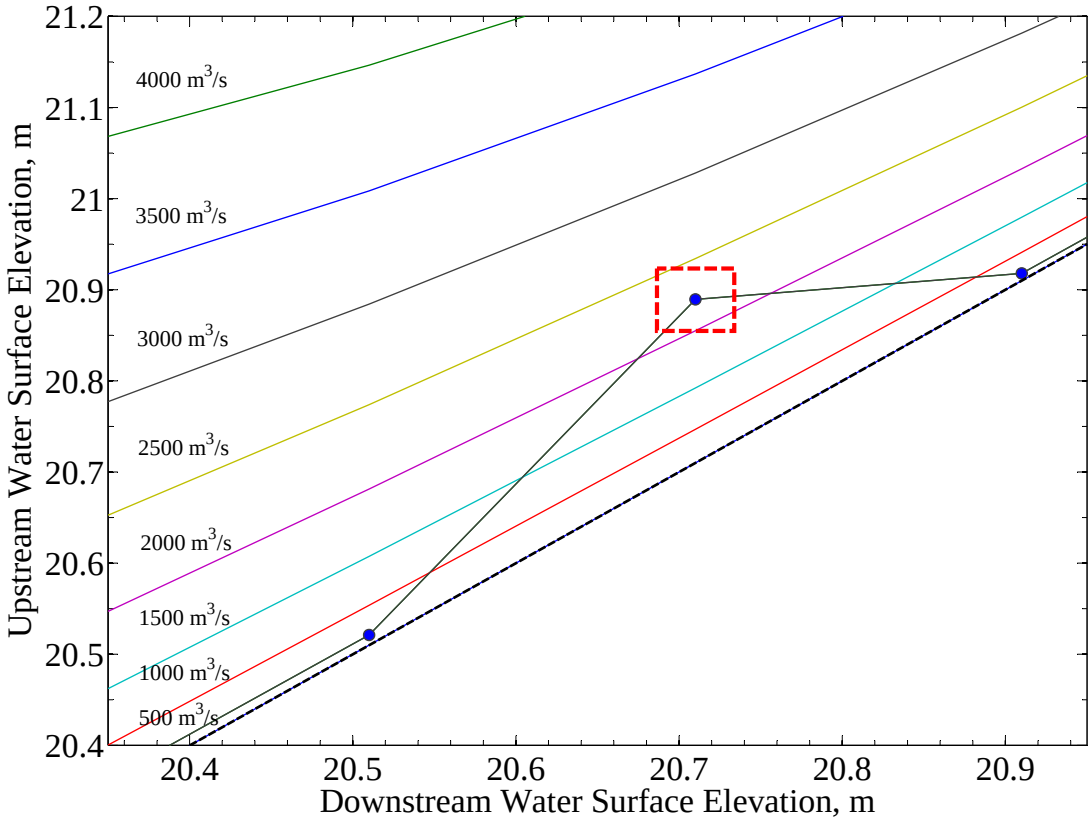

Figure 2.12: Example of instability problem at 500 m^3/s HPC

2.5.4 Performance Graph Junctions

Simulating unsteady flows through river network junctions require computationally expensive iterative schemes or simplifications such as those used in current one-dimensional unsteady hydraulic models (e.g. HEC-RAS, MIKE11, etc.). Even so, in many occasions, the iterative schemes may not converge and in some cases may produce numerical instabilities. During this research, a new method for approximating junction head-losses has been tested. Standard junction conditions typically require water surface elevation compatibility via energy balance, momentum balance, and conservation of mass. As previously stated, so long as the upstream and downstream ends of a channel reach have

approximately one-dimensional velocity profiles, then the Performance Graph assumptions are satisfied. The head-loss terms can be accounted for by projecting the nearest cross-section of each branch that displays near one-dimensional flow up to the original junction, as an additional reach (e.g. Fig. 2.13). The additional reaches are treated as standard PG reaches.

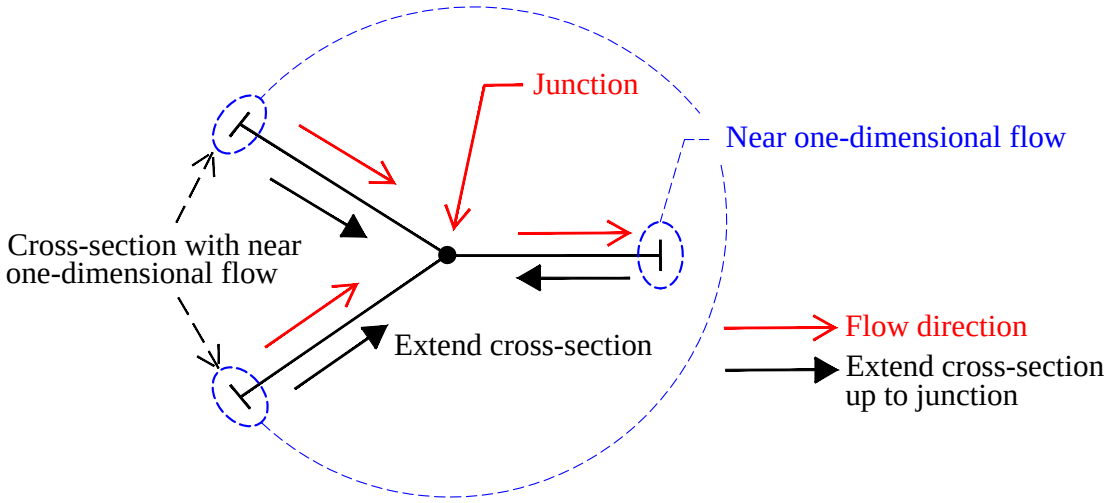

Figure 2.13: Performance graph junction illustration

2.6 Results

Generating Performance Graphs requires the computation of gradually varied flow scenarios within a given reach. Each curve of the performance graph consists of a series of GVF hydraulic simulations through a range of fixed downstream water stages, hence, each performance graph is composed of hundreds, potentially thousands of simulations dependent on desired resolution. The TELEMAC-2D simulations were conducted in a batch-style manner utilizing the Parallel Computing Toolbox within MATLAB and also using parallel batch scripts. Given that each hydraulic GVF simulation is solved independently of one another, embarrassingly parallel computation techniques can be employed (e.g. parametric sweeps, high performance computing clusters, etc.). As an example, Figures 2.14 and 2.15 show the 2D-HPG and 2D-VPG for Reach US-3 in the

Fraser River; for display purposes, some of the HPCs were removed intentionally.

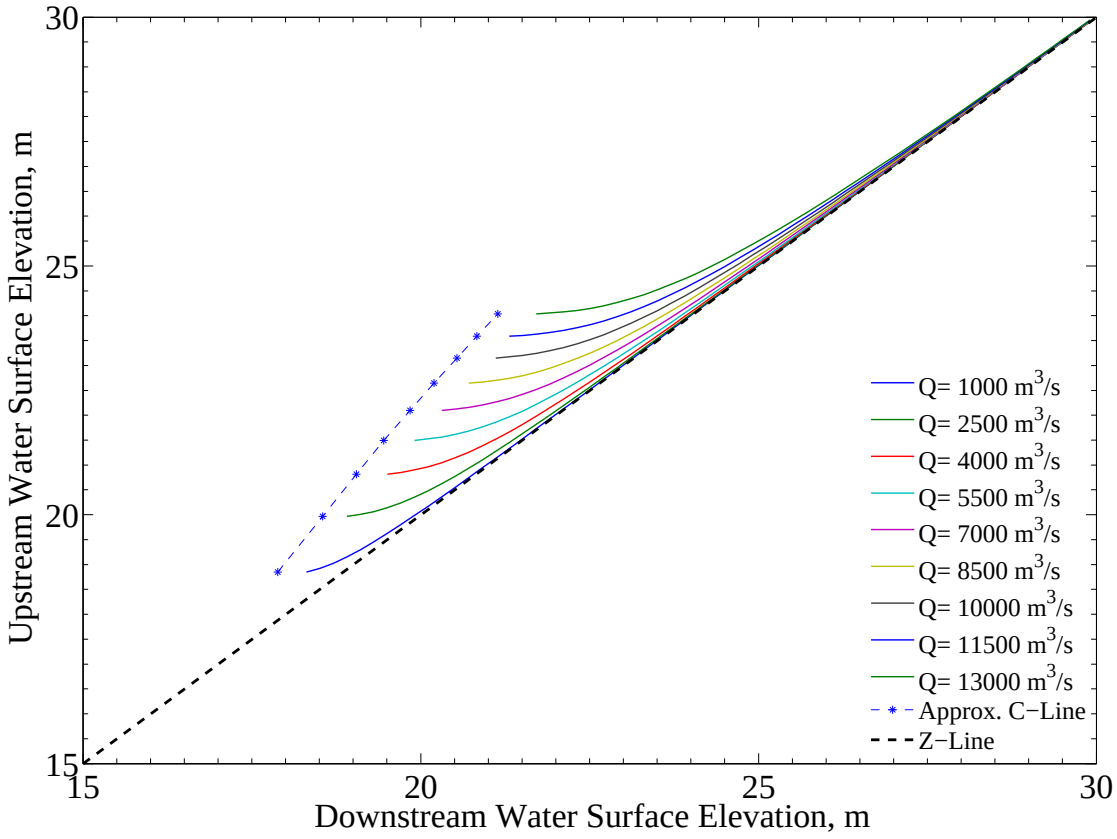

Figure 2.14: 2D-Hydraulic Performance Graph for reach US-3 of the Fraser River system

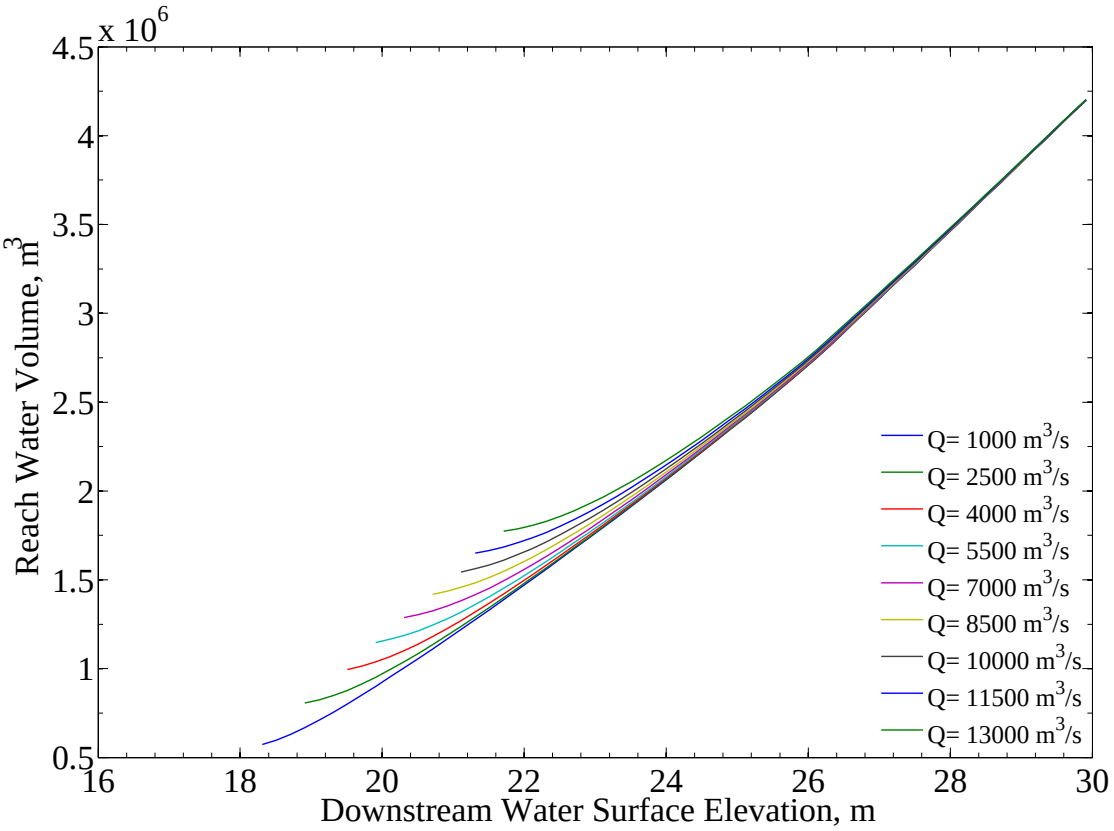

Figure 2.15: 2D-Volumetric Performance Graph for reach US-3 of the Fraser River system

A comparison between HPCs generated from TELEMAC-2D and the Steady 1D HEC-RAS model has been made for three specified discharges through reach US-3 of the Fraser River system and are shown in Figure (2.16). The relative difference in resulting water depths between the 1D and 2D HPCs are computed using Eq. (2.19). Each GVF simulation was performed using the same geometry and fixed downstream water surface elevations for both models. The relative errors in resulting depths are shown in Figure (2.17). Results from Figure (2.17) suggest that the individual HPCs yield a difference in computed depths of $\pm$ 0.1-4.0%, with discrepancies increasing as discharge rises. In general, the 1D HEC-RAS simulations result in higher upstream water surface elevation (WSE) values for each scenario suggesting that for each flow scenario through reach

US-3, TELEMAC-2D predicts higher headlosses than the 1D HEC-RAS model.

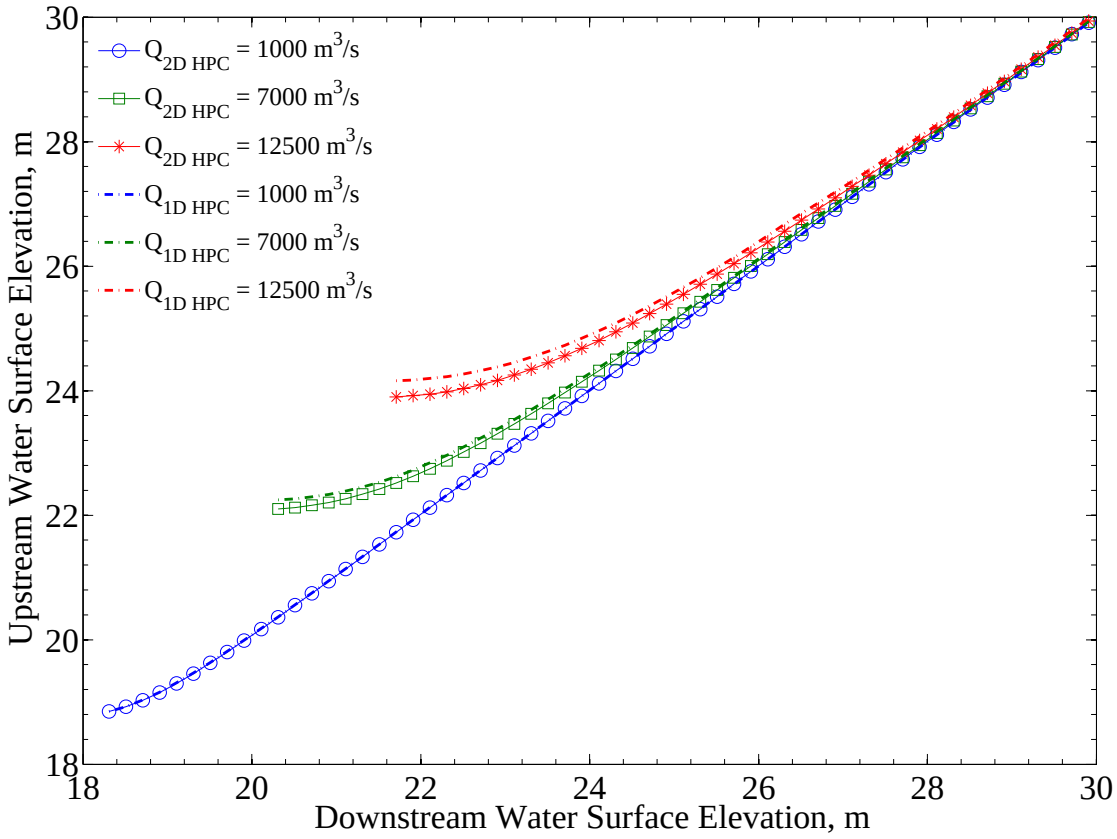

Figure 2.16: Comparison of one-dimensional HEC-RAS and two-dimensional HPCs for reach US-3

$$\mathrm{E}_{h_{\text{2D-PG}}}(\%) = 100\left(\frac{h_{\text{2D-PG}} - h_{\text{1D-PG}}}{h_{\text{2D-PG}_{\max}} - h_{\text{2D-PG}_{\min}}}\right) \tag{2.19}$$

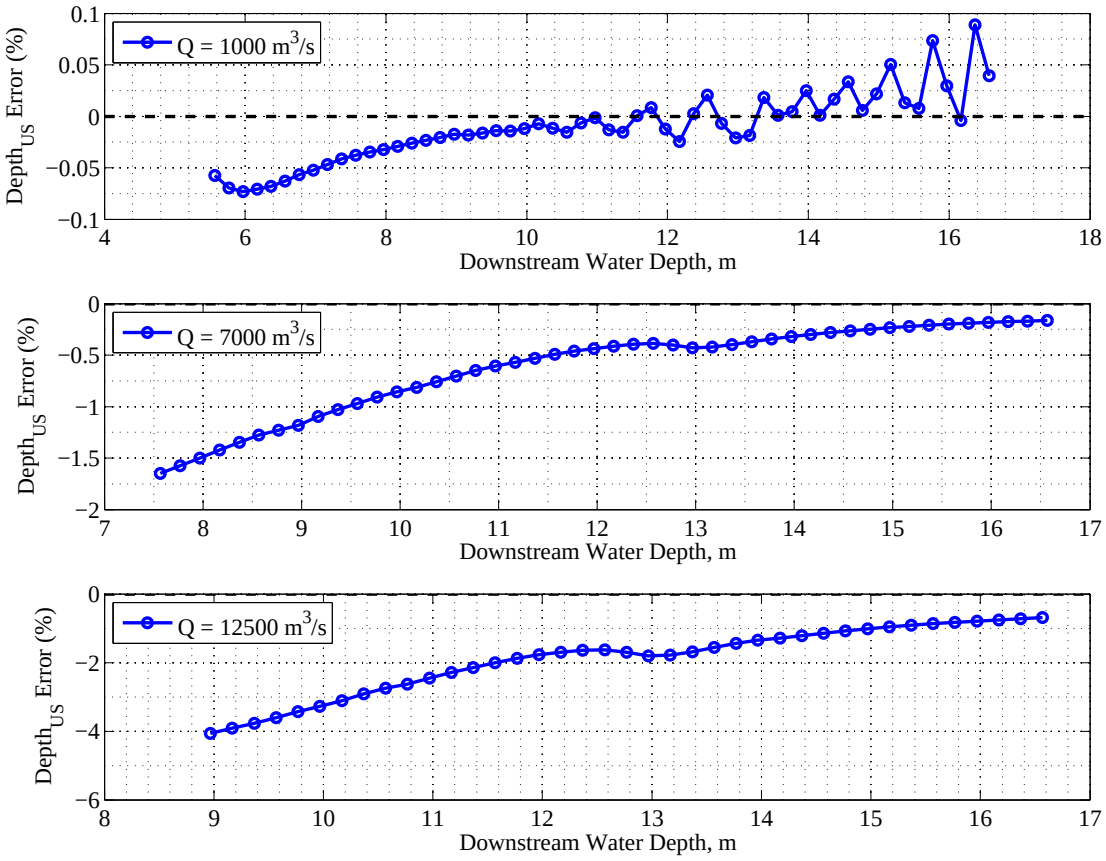

Figure 2.17: Percent difference in water depths when comparing selected Hydraulic Performance Curves from reach US-3 for one-dimensional HEC-RAS and two-dimensional PG generation

Two dimensional performance graphs (2D-PGs) were generated for all reaches in the Fraser River application and assembled for unsteady flow routing as inputs for the OSU-Rivers model. OSU-Rivers assembles and solves a nonlinear system of equations based on information summarized in the reaches HPGs and VPGs, continuity and compatibility of water stages at junctions, and the system's initial and boundary conditions (Leon et al., 2013a). Figure (2.18) shows the results of hydraulic routing of a flood-wave by the OSU-Rivers unsteady flow routing model, TELEMAC-2D hydrodynamics model, and the Unsteady HEC-RAS model. The comparison in Fig. (2.18) shows that similar

results are achieved when contrasting the OSU-Rivers outflow hydrograph to that of the TELEMAC-2D model. The results indicate that 2D models may not be necessary for modeling water stage and flow discharge in rivers when the flow is inside the main channel.

The resulting CPU times for each model are shown in Table 2.4. CPU time calculation included preprocessing and computational engine times, while post-processing was excluded. As can be seen from Table 2.4, the computational efficiency of OSU-Rivers when compared to TELEMAC-2D is significant.

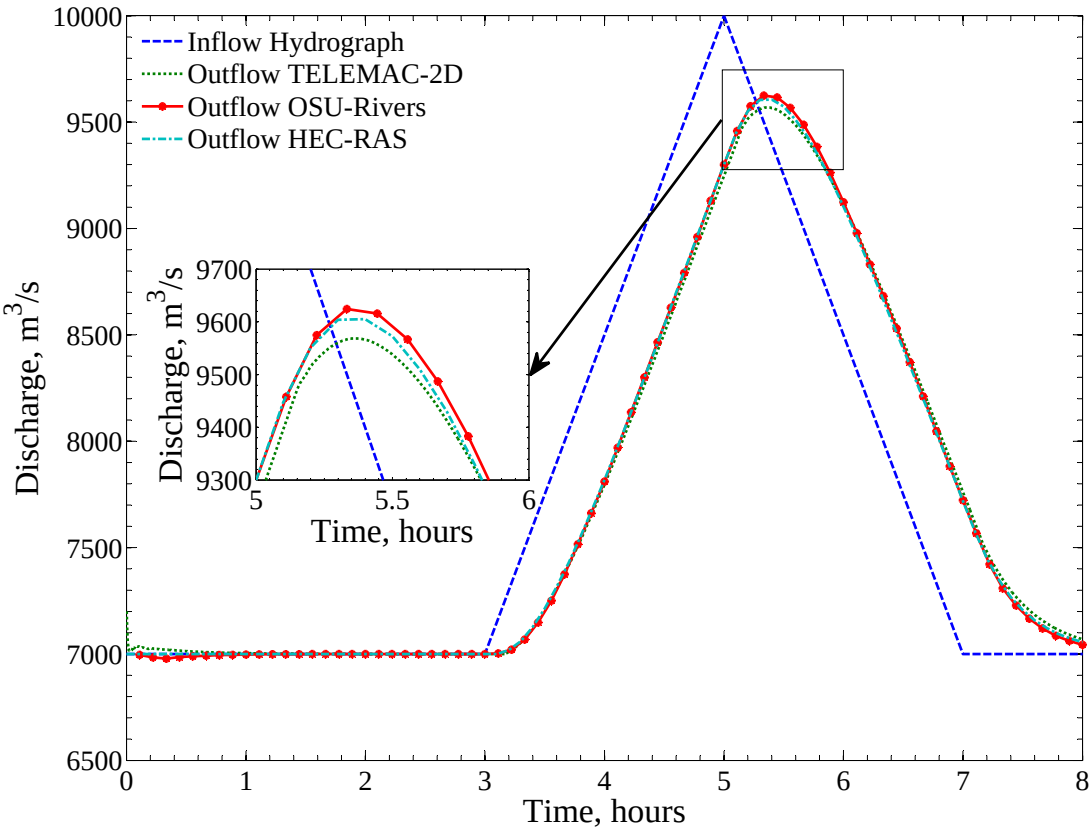

Figure 2.18: Comparison between unsteady TELEMAC-2D, OSU-Rivers, and HEC-RAS outflow hydrographs

Table 2.4: Comparison of CPU time for unsteady flow routing test case

Model	Δt (s)	CPU Time (s)
TELEMAC-2D	1.0	14305
OSU-Rivers	400	0.56
HEC-RAS	360	5.41

2.7 Conclusions

This paper investigated the applicability of using a depth-averaged two-dimensional hydrodynamics model for the construction of performance graphs and their application to unsteady flow routing. The TELEMAC-2D model was used to simulate the array of gradually varied flow profiles necessary to construct performance graphs for a looped river system, divided into 18 reaches. The key findings are as follows:

1. 1D-, or 2D-Computational Fluid Dynamics (CFD) programs can be used to generate PGs. Recent advancements in computer hardware and parallel programming enables batch simulations of complex CFD simulations.

2. When the river flow stays within the main-channel, the results of 1D-PGs and 2D-PGs produce similar results. If flow exceeds the bank and enters the flood-plain however, 2D-PGs may be required.

3. Computation efficiency of the OSU-Rivers model compared to TELEMAC-2D is significant. OSU-Rivers also obtains comparable results to TELEMAC-2D in water stage and flow discharge.

2.8 Acknowledgments

The authors gratefully acknowledge the financial support of the Bonneville Power Administration of the U.S. Department of Energy under award number TIP#258. The authors would also like to thank Northwest Hydraulic Consultants (NHC), Vancouver, B.C., for providing the bathymetric data used for this study.

2.9 Notation

The following symbols are used in this paper:

WSE	=	water surface elevation;
HPG	=	hydraulic performance graph;
VPG	=	volume performance graph;
HPC	=	hydraulic performance curve;
PG	=	performance graph;
US	=	upstream reach;
RB	=	right branch;
LB	=	left branch;
DS	=	downstream;
ADCP	=	acoustic doppler current profiler;
GCI	=	grid convergence index;
Q	=	discharge;
A	=	cross-sectional area;
t	=	time;
g	=	gravitational acceleration;
h	=	flow depth;
S_f	=	friction slope;
S_o	=	bed slope;
θ	=	angle between channel bed and horizontal plane;
n	=	Manning's roughness;
V	=	depth averaged velocity vector;
Z_s	=	water stage;
ν_T	=	turbulent eddy viscosity;
k	=	turbulent kinetic energy;
ϵ	=	turbulent dissipation;
V_*	=	shear velocity;
C_f	=	dimensionless friction coefficient;
F_x, F_y	=	source terms accounting for boundary friction;
ρ	=	density;
$\dot{Q}$	=	rate of heat added to the system;
$\dot{W}_{shear}$	=	shear work done on system;
CS	=	control surface;
$\dot{m}$	=	mass flowrate;
p	=	pressure;
Δt	=	time step

Subscripts

ds = downstream end;

us = upstream end;

x = x direction component;

y = y direction component;

i = tensor notation index;

Superscripts

n = discrete-time index

Chapter 3: A Framework for Propagation of Uncertainty in River Systems

3.1 Introduction

The prediction and control of reservoir systems is important for many reasons, including flood control, hydropower production, and irrigation. Uncertainties arise via upstream inflows, weather forecasts, imprecise measurements of water levels, and hydropower demands. The resulting PDE-constrained optimal control problem is a complex task involving stochastic inputs and objectives, probabilistic constraints, and nonlinear evolution equations imposed on massive domains. Both the optimization component and the uncertainty quantification require numerous forward simulations of the system. We focus here on the forward problem and limit the discussion to uncertain inputs.

Uncertain inflows were introduced into a multi-reservoir network using a linear, stochastic perturbation of an expected inflow hydrograph in (Leon et al., 2012). A *polynomial chaos expansion* (PCE) (Ghanem and Spanos, 1991; Xiu and Karniadakis, 2002; Chen et al., 2005) of the outflow was computed using a *Stochastic Collocation* approach, see e.g. (Mathelin et al., 2005; Xiu and Hesthaven, 2005; Babuška et al., 2007). In the current work, we investigate additional aspects of this general approach to uncertainty quantification in reservoir modeling. In particular, we assume that predictions of inflow hydrographs (ensemble forecasts) come from various sources, each of which possibly with its own probability of being realized. We wish to translate this discrete set of data into a continuous random framework amenable to PCE. Additionally, we wish to quantify the possible errors in the approximation resulting from this translation. We can then effectively reduce the dimension of the random input space to a manageable number with metrics to estimate the error induced by the approximate subspace. We again use Stochastic Collocation in computing modes of the uncertain solution, in order to allow efficiencies in the deterministic forward simulation to be exploited.

Lastly, in order to further reduce the computational burden of the uncertain forward problem, we suggest an approach for decomposing the problem into subdomains which can be used in a parallelization of the deterministic forward simulation. Combined, the methods which we describe below allow for efficient, and adaptive, determination of stochastic solutions to the uncertain multi-reservoir river system.

3.2 Governing equations

In the following we present an unsteady flow routing (river system flow dynamics). Due to space limitations we consider only one-dimensional models. In a one-dimensional context, under a deterministic assumption, unsteady flows in open-channels are typically represented by the Saint-Venant equations, a pair of one-dimensional partial differential equations representing conservation of mass and momentum for a control volume, which is shown in conservative differential form in Equations (3.1) and (3.2)

$$\frac{\partial A}{\partial t} + \frac{\partial Q}{\partial x} = 0 \tag{3.1}$$

$$\frac{1}{A}\frac{\partial Q}{\partial t} + \frac{1}{A}\frac{\partial}{\partial x}\left(\frac{Q^2}{A}\right) + g\cos(\theta)\frac{dy}{dx} - g(S_0 - S_f) = 0. \tag{3.2}$$

In these equations, x = distance along the channel in the longitudinal direction; t = time; Q = discharge; A = cross-sectional area; y = flow depth normal to x; θ = angle between the longitudinal bed slope and a horizontal plane; g = acceleration of gravity; S_0 = bed slope and S_f = friction slope. Appropriate initial and boundary conditions are required to close the system. Due to the presence of non-linear terms in Equation (3.2), there is in general no closed-form solution. The equations are therefore solved numerically. In a network involving numerous branches, the system of equations that must be solved becomes extremely large and the application of the full Saint-Venant equations becomes inefficient for real-time operation because of the significant computational requirements and error accumulations (Hoy and Schmidt, 2006b).

Instead we use the performance graphs approach described in (Leon et al., 2013a). The method solves a reduced non-linear system of equations to perform the hydraulic routing of the system. The equations are assembled based on information in the reaches and nodes summarized in appropriate performance graphs formed from high fidelity, pre-computed solutions. These are combined with continuity and compatibility of water stages at junctions, and the system's initial and boundary conditions. Due to the pre-computation of solutions, efficiencies cannot be realized if the simulator must adjust to incorporate uncertainty, therefore we seek a *non-instrusive* uncertainty framework.

3.3 Uncertainty framework

In the current work, only the stream inflows (external sources) are assumed to be completely stochastic. Other uncertain quantities are correlated to the uncertainty of the stream inflows using the dynamics of the system. For the efficient computation of the uncertainty components, rather than doing random sampling of the input distributions, we propose to explicitly model the random space (via random variables and processes) and perform a generalized Polynomial Chaos (gPC) representation (Ghanem et al., 2005; Ghanem and Doostan, 2006; Xiu and Karniadakis, 2002; Xiu, 2010).

Convergence of polynomial chaos methods can be shown to be exponential in the number of basis functions (Xiu and Karniadakis, 2002). Due to the polynomial representation, these integrals may be computed exactly, however this approach in general leads to a large coupled system of equations and this new system must be discretized in space and time (e.g., an *intrusive method* which changes the system to be solved). Instead, we wish to utilize a well-developed forward solution methodology based on performance graphs (Leon et al., 2013a). We therefore employ the Stochastic Collocation (Babuška et al., 2007; Xiu and Hesthaven, 2005) method for the computation of coefficients of the PCE, a *non-intrusive method* which we couple with the performance graphs implementation in OSU Rivers (Leon et al., 2013a).

Polynomial Chaos has been studied in computational fluid dynamics by numerous investigators (e.g., Xiu and Karniadakis, 2002; Chen et al., 2005; Knio and Le Maître, 2006; Hou et al., 2006). The *non-intrusive* Stochastic Collocation method was introduced in the computational fluid dynamics literature in (Mathelin et al., 2005).

Stochastic Collocation was successfully applied to a non-linear model for incompressible flow and heat transfer around an array of circular cylinders based on the two-dimensional Reynolds-averaged Navier-Stokes equations (Constantine et al., 2009). The uncertainty was introduced through boundary conditions in a steady-state model.

A network of human arteries was considered in (Xiu and Sherwin, 2007) where weakly non-linear 1D equations of pressure and flow wave propagation were used as a model in each section of compliant vessels. While a network was considered, with mass balance interface conditions similar to the model described in the current work, the uncertain quantities were restricted to the geometric and physical properties of the artery, not inflows or boundary conditions. The study on human arteries did demonstrate the

feasibility of Stochastic Collocation on a physiologically realistic network of 37 branches.

The proposed framework can be used for any complex river network. For illustration purposes, consider the sample network system presented in Figure 3.1 from (Leon et al., 2012). This dendritic-looped network consists of eight river reaches, two reservoirs and three boundary conditions (one inflow hydrograph, one stage hydrograph and one rating curve). The (nonlinear) relationship between variables $\vec{X} =$

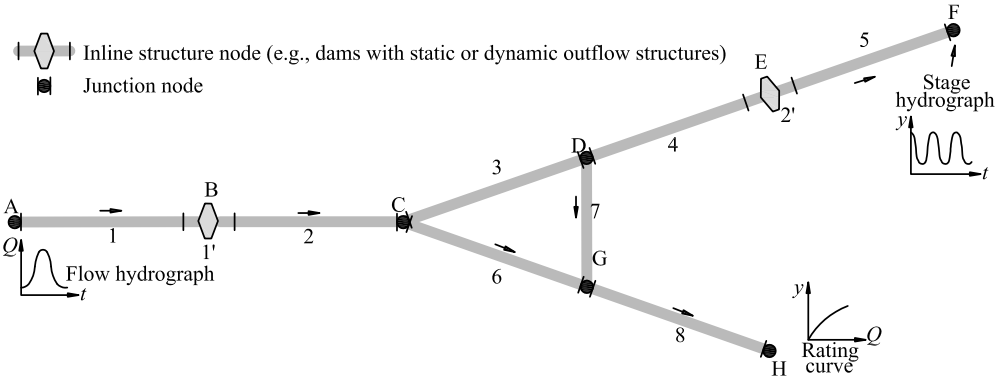

Figure 3.1: Schematic of a simple network system from (Leon et al., 2012)

$[y_{d_1} \dots y_{d_8}, Q_{u_1} \dots Q_{u_8}, Q_{d_1} \dots Q_{d_8}]$ (water stages y and flow discharges Q upstream and downstream of each river reach) on each timestep is represented using the performance graphs approach described in (Leon et al., 2013a).

In what follows we describe the method we use to introduce the uncertainty into the system. Let $(\Omega, \mathcal{F}, P)$ be a complete probability space, where Ω is the set of outcomes, $\mathcal{F} \subset 2^{\Omega}$ is a σ-algebra of events and $P : \mathcal{F} \to [0, 1]$ is a probability measure. Assume that the initial inflow function Q_{u_1} can be described as a function of finite number N_{rv} of independent random variables $\{\xi_k\}_{k=1}^{N_{rv}}$, i.e.

$$Q_{u_1}(t, \omega) = Q_{u_1}(t, \xi_1(\omega), \xi_2(\omega), \dots, \xi_{N_{rv}}(\omega)). \tag{3.3}$$

Let $\rho_k : \Gamma_k \to \mathbb{R}^+$, $k = 1, 2, \dots, N_{rv}$, denote the probability density function of the random variable ξ_k, with the image $\Gamma_k = \xi_k(\Omega) \subset \mathbb{R}$, $k = 1, 2, \dots, N_{rv}$. If the random variables $\{\xi_k\}_{k=1}^{N_{rv}}$ are independent then the joint probability density function ρ is given

by the product of the corresponding densities

$$\rho(\mathbf{z}) = \prod_{k=1}^{N_{rv}} \rho_k(z_k), \quad \mathbf{z} \in \Gamma, \quad z_k \in \Gamma_k, \tag{3.4}$$

where $\Gamma = \prod_{k=1}^{N_{rv}} \Gamma_k \subset \mathbb{R}^{N_{rv}}$ is a support of the joint density function ρ. The introduction of uncertainty through the boundary conditions allows us to consider model (3.1) and (3.2) in the form of stochastic equations, i.e., find $Q : \mathbb{R} \times [0, T] \times \Gamma \to \mathbb{R}$ such that for all $\mathbf{z} \in \Gamma$, (3.1) and (3.2) hold subject to appropriate initial and boundary conditions, including $Q(x = 0, t, \omega) = Q_{u_1}(t, \omega)$.

3.4 Karhunen-Loève representation of the inflow function

In what follows we assume that the logarithm of the inflow function Q_{u_1} can be represented as a Gaussian process. This is quite a strong assumption although the general uncertainty framework we use can be adjusted if it is violated.

In order to obtain a representation for the inflow function Q_{u_1} we use the following procedure (Babuška et al., 2003):

1. Suppose we have M realizations of the inflow function $\{Q_{u_1,i}\}_{i=1}^{M}$ measured at time points $\{t_j\}_{j=0}^{n}$, where $t_j = t_0 + jh$, $h = \dfrac{T - t_0}{n}$, $j = 1, \ldots, n$, and $[t_0, T]$ is a time interval of interest. By $Q_{u_1,i}(t_j)$ we denote the value of the i-th realization of the inflow function at the time point t_j. Let $L_i(t_j) = \ln Q_{u_1,i}(t_j)$ denote the logarithm of the inflow at t_j, and $L(t) = \ln Q_{u_1,i}(t)$.

2. Then we compute the sample mean vector $\bar{L} = (\bar{L}_1, \bar{L}_2, \ldots, \bar{L}_n)'$ and an $(n \times n)$ covariance matrix C with elements $c_{j,k}$ of the transformed inflows using the following formulas

$$\bar{L}_j = \bar{L}(t_j) = \frac{1}{M} \sum_{i=1}^{M} L_i(t_j), \quad c_{j,k} = \frac{1}{M-1} \sum_{i=1}^{M} (L_i(t_j) - \bar{L}_j)(L_i(t_k) - \bar{L}_k). \tag{3.5}$$

3. It follows that $L(t)$ can be represented in the form of its infinite series representa-

tion, called the Karhunen-Loève expansion (Xiu, 2010),

$$L(t) = \bar{L}(t) + \sum_{k=1}^{\infty} \sqrt{\lambda_k}\psi_k(t)\xi_k, \tag{3.6}$$

where $\{\lambda_k, \psi_k\}_{k=1}^{\infty}$ are the eigenpairs of the integral equation

$$\lambda\psi(t) = \int_{t_0}^{T} C(s,t)\psi(s)ds, \tag{3.7}$$

with $C(t_j, t_k) = c_{j,k}$; and $\{\xi_k\}_{k=1}^{\infty}$ is a sequence of uncorrelated random variables with mean 0 and variance 1 defined by

$$\xi_k = \frac{1}{\sqrt{\lambda_k}} \int_{t_0}^{T} [L(t) - \bar{L}(t)]\psi_k(t)dt, \quad k \geq 1. \tag{3.8}$$

We assume that the eigenvalues are arranged in decreasing order, that is, $\lambda_1 > \lambda_2 > \lambda_3 > \cdots$. In the case L is a Gaussian random process, $\{\xi_k\}_{k=1}^{\infty}$ are independent and identically distributed normal random variables with mean 0 and variance 1.

Then the inflow function Q_{u_1} has the following representation

$$Q_{u_1}(t) = \exp\left(\bar{L}(t) + \sum_{k=1}^{\infty} \sqrt{\lambda_k}\psi_k(t)\xi_k\right). \tag{3.9}$$

From the practical point of view it is not possible to use the infinite series representation of Q_{u_1}. The truncated representation is used instead

$$Q_{u_1}(t) \approx Q_{N_{rv}}(t) = \exp\left(\bar{L}(t) + \sum_{k=1}^{N_{rv}} \sqrt{\lambda_k}\psi_k(t)\xi_k\right). \tag{3.10}$$

The number of terms N_{rv} in the truncated representation can be chosen in different ways. One may use a fact that $\sum_{n=1}^{\infty} \lambda_n = \int_{t_0}^{T} C(s,s)ds$. Based on this criteria we can choose the number of terms that would capture the major part of the variability. Another way to determine N_{rv} is to look at the convergence rate of the eigenvalues and get rid of those that are close to 0, or insignificant in comparison with the first eigenvalue. For

example, we can include the eigenvalues λ_n that satisfy

$$\lambda_n < a\lambda_1 \tag{3.11}$$

for some predefined constant $0 < a < 1$. In some sense a can be treated as a tolerance. A different perspective on this problem is given in the next section.

3.5 Distributional sensitivity

The representation of the random field in terms of the truncated series has its own features distinct from the original process. If the random process of interest is Gaussian, e.g., the logarithm of the inflow, then the truncated KL expansion is a random process represented as a linear combination of several standard Gaussian random variables. If the random process is not Gaussian, the representation of the process in the form of its Karhunen-Loève expansion becomes harder to obtain. The procedure has to involve the estimation of the distribution of the random coefficients in the series representation. In general, for non-Gaussian processes there may not be enough data to accurately specify the distribution of the random variables. This creates additional sources of uncertainty which in this case relate to the lack of data and may not be easily overcome.

In the work (Narayan and Xiu, 2011), the authors describe a distributional sensitivity analysis as a way to reduce epistemic uncertainty. The idea is to quantify the effect of the particular distribution of the random variables on the distribution or statistical moments of the solution. The random variables with large distributional sensitivity would require more attention and effort to approximate their distribution while the distribution of random variables with small distributional sensitivity can be approximated at lower computational expense. The distributional sensitivity allows one to obtain an additional rank (aside from the eigenvalues) of the random variables in the KL expansion based on their actual effect on the quantities of interest. This, for example, can suggest an increase or decrease in the number of collocation (or quadrature) points used to approximate expectations in a particular random dimension.

For simplicity of exposition we assume that the solution Q_{d_8} depends on the random vector $\vec{\xi} = (\xi_1, \xi_2, \ldots, \xi_{N_{rv}})$ through the boundary conditions imposed as stream inflow Q_{u_1}. We assume that vector $\vec{\xi}$ has a joint density function ρ_1. In our experiments ρ_1 is a

joint Gaussian density, i.e. each component of the vector $\vec{\xi}$ has normal distribution with mean zero and variance 1. To quantify the sensitivity of the solution Q_{d_8} to the distribution of the random variables $\{\xi_k\}_{k=1}^{N_{rv}}$ we consider the following discrete distributional sensitivity

$$\mathrm{DS}_{\mathcal{E}}[\rho_1, \rho_2](Q_{d_8}) = \frac{\|\mathcal{E}_{\rho_1}(Q_{d_8}) - \mathcal{E}_{\rho_2}(Q_{d_8})\|}{d(\rho_1, \rho_2)}, \tag{3.12}$$

where $\mathcal{E}_\rho(Q_{d_8})$ is a quantity of interest associated with Q_{d_8}, for example, mean or variance, with respect to the probability density ρ; ρ_2 is a perturbation of the density ρ_1; $d(\rho_1, \rho_2)$ is a measure of distance between two densities, for example, it can be an L^1 norm.

It is worth mentioning that ρ_1 and ρ_2 do not necessarily share the common parameterization. The distributional sensitivity depends only on the densities ρ_1 and ρ_2, so, in general, it does not matter what numerical methods are used to approximate the solution Q_{d_8}. The calculation of the distributional sensitivity is post-processing step, no additional solutions are required. The moments can be obtained by using the Stochastic Collocation method (described in the following section). For the moments with respect to the density ρ_1 one can use the usual collocation points and weights; for the moments with respect to the perturbed density ρ_2 one can use the same collocation points with weights scaled by the ratio ρ_2/ρ_1 evaluated at the given collocation point.

3.6 Polynomial Chaos Expansion

To solve the problem (3.1) and (3.2) in the stochastic context we use the generalized Polynomial Chaos Expansion (PCE). To illustrate the idea of the proposed uncertainty approach, the following example is presented. Consider the quantity Q_{u_1} representing flow discharges upstream of reach 1 in Figure 3.1. We assume that a prediction of this quantity $\mu_{Q_{u_1}}(t)$ is given and treated as an expectation. Additionally we assume that based on the previous history or some additional data we can construct an uncertainty envelope around this prediction using the KL expansion, for example,

$$Q_{u_1}(t) = \mu_{Q_{u_1}}(t) + \sum_{k=1}^{N_{rv}} \sqrt{\lambda_k}\psi_k(t)\xi_k. \tag{3.13}$$

We can think about equation (3.13) as a PCE of the random input when the polyno-

mials of degree 1 are used. In a stochastic Galerkin method one seeks to determine the coefficients of a PCE of each component of the solution vector $[y_{d_1}, \ldots, y_{d_8}, Q_{u_1}, \ldots, Q_{u_8}, Q_{d_1}, \ldots, Q_{d_8}]$, or some function of the solution vector. To do this, one may take a Galerkin projection of the original system against the polynomial chaos basis functions, with these expansions substituted in for the solution quantities.

For example, consider the most downstream reach, Q_{d_8}. Its representation in terms of a degree p expansion

$$Q_{d_8}^P(t, \vec{\xi}) = \sum_{i=0}^{M_p} v_i(t)\phi_i(\vec{\xi})$$

where $\vec{\xi} = (\xi_1, \xi_2, \ldots, \xi_{N_{rv}})$ is a vector of random variables in the representation of Q_{u_1}, M_p is a number of basis functions, $\{\phi_i\}_{i=0}^{M_p}$ are the N_{rv}-variate orthogonal polynomial functions of degree up to p. The maximum possible number of polynomial basis functions is $(N_{rv}+p)!/(N_{rv}!p!)$. Note that the final number of basis functions depends if the same degree polynomials are used for the approximation in each random dimension. Corresponding to the normal distribution of each components of $\vec{\xi}$, the orthogonal polynomials ϕ_i are chosen as tensor products of univariate Hermite polynomials.

Since the relationship between Q_{u_1} and Q_{d_8} is clearly nonlinear, more than two basis functions will be required for accurate representation of Q_{d_8}. Depending on the importance of the particular component of the random vector $\vec{\xi}$, determined, for example, by distributional sensitivity, a different level of approximation can be chosen in the kth random direction associated with ξ_k, $k = 1, \ldots, N_{rv}$.

Each PCE coefficient can be found as an expectation

$$v_i(t) = E[Q_{d_8}(t, \vec{\xi})\phi_i(\vec{\xi})] = \int_\Gamma Q_{d_8}(t, \mathbf{z})\phi_i(\mathbf{z})\rho(\mathbf{z})d\mathbf{z}. \tag{3.14}$$

The computation of the coefficients (3.14) can be done efficiently with the use of the Stochastic Collocation method (Babuška et al., 2007).

The outline of the Stochastic Collocation method and PCE is given below:

1. Choose a set of collocation points $(\mathbf{z}_j, w_j)$, $\mathbf{z}_j \in \Gamma$, where $\mathbf{z}_j = (z_{j,1}, z_{j,2}, \ldots, z_{j,N_{cp}})$ is a j-th node and w_j is its corresponding weight, $j = 1, \ldots, N_{cp}$. We suggest to use a sparse grid since it can greatly reduce the computational expense.

2. For each $j = 1, \ldots, N_{cp}$ determine the inflow function $Q_{u_1,j}$ and solve the corre-

sponding (deterministic) system of equations (3.1) and (3.2), in parallel, to obtain the flow $Q_{D_8,j}$.

3. Approximate the PCE coefficients

$$v_i(t) = \mathbb{E}[Q_{d_8}(t,\vec{\xi})\phi_i(\vec{\xi})] \approx \sum_{j=1}^{N_{cp}} w_j Q_{d_8}(t,\mathbf{z}_j)\phi_i(\mathbf{z}_j). \tag{3.15}$$

4. Finally, construct the N_{rv}-variate, pth-order PCE approximation of the solution

$$Q_{d_8}^p(t,\vec{\xi}) = \sum_{i=0}^{M_p} v_i(t)\phi_i(\vec{\xi}). \tag{3.16}$$

The same coefficients v_i can be used to approximate the first two moments of the solution, e.g.

$$E[Q_{d_8}(t,\vec{\xi})] \approx v_0(t), \quad \mathrm{Var}[Q_{d_8}(t,\vec{\xi})] \approx \sum_{i=0}^{M_p} v_i(t)^2. \tag{3.17}$$

Gaussian quadrature applies efficiently to functions which can be represented as $g(\vec{\xi})W(\vec{\xi})$ where $g(\vec{\xi})$ is well-approximated by a polynomial. The nodes $\vec{\xi}_j$ of the quadrature rule are the roots of a predetermined orthogonal polynomial (by choice of distribution) in the support of ρ, and the method has the highest degree of precision possible. Stochastic Collocation requires only solutions of the deterministic system evaluated at the fixed points $\{\vec{\xi}_j\}_{j=1}^{N_{cp}}$ of the random vector $\vec{\xi}$. Upon computation of the expansion coefficients for the quantities of interest, we have an analytical representation of a surrogate of the stochastic solution in polynomial form. This allows, among other things, various solution statistics to be easily obtained, such as expected value (or higher order modes), or parametric sensitivities (Xiu and Sherwin, 2007). The PCE for any function f of output (non-linear, non-smooth or even discontinuous) may be easily constructed as follows

$$v_i(t) = \mathbb{E}[f(\vec{X}(t,\vec{\xi}))\phi_i(\vec{\xi})] \approx \sum_{j=1}^{N_{cp}} w_j f(\vec{X}(t,\vec{\xi}_j))\phi_i(\vec{\xi}_j).$$

In practice, only desired functions of the solution of the system need to be represented explicitly. For instance, in a multi-objective optimal control framework, the outflows and

water stages at the reservoirs may be the actual quantities of interest. The above example can be restated via a mapping from the solution quantities to the desired quantities. It is important to note that this mapping need not be linear, nor need it even be continuous, as demonstrated in (Marzouk and Xiu, 2009), however in the latter case exponential convergence is sacrificed in favor of algebraic.

3.7 Computational Issues

As described above there are several aspects of the problem for which the computations can be quite expensive. In this simple model we have introduced only a single random inflow, while a realistic model of a complex river network might require several. Each inflow should be modeled with at least one random dimension. Taking into account all inflows would imply a dependence of the solution on a large number of variables. Computation of modes of a stochastic solution thus requires high dimensional integrations, in addition to the fact that each single deterministic simulation is already expensive.

In the above we have described two complementary approaches for reducing the computational effort required to obtain solutions to the uncertainty propagation problem. As stochastic collocation is easily parallelizable, efficiencies can be made in a straightforward manner. However, current massively parallel architectures are not well-suited for this type of distributed computing as each computational node would need to hold the entire problem in memory, a more difficult task considering that the performance graphs approach requires thousands of solutions to be stored to be used in an interpolation scheme. In fact, if high precision is required in these precomputed solutions, it may not be feasible to hold the entire performance graphs collection in memory on high memory workstations. Therefore a fine-grained parallelism should be used, based on domain decomposition strategies (Gunzburger et al., 1999). In this manner, one computational node would be responsible for one or possibly several reaches of the network, and would need to communicate with two other nodes (those with reaches that share interfaces) on each performance graph time interval (not the time step used in the computation of the performance graph) in order to converge iteratively to satisfy appropriate interface conditions.

The performance graph approach lends itself to this type of decomposition due to the fact that solutions for each reach on a reference time interval are stored on only one node,

and the entire system solution at the previous time interval determines the solution on that reach for the next time interval. Further, the non-intrusive nature of the Stochastic Collocation method allows efficiencies in deterministic solvers to be realized. The level of fine-grained splitting would be determined by memory constraints and desired precision of solutions, and would be used in addition to the coarse-grained parallelism allowed by Stochastic Collocation. The detailed formulation, analysis and implementation of this procedure will be the topic of a future paper.

3.8 Numerical Experiments

For our simulation experiments we use the river system illustrated on the Figure 3.2. We assume that forecast of the inflow Q_{u_1} is given for reach 1. We wish to calculate the expected outflow $Q_{d_{25}}$ at reach 25, along with a quantification of uncertainty.

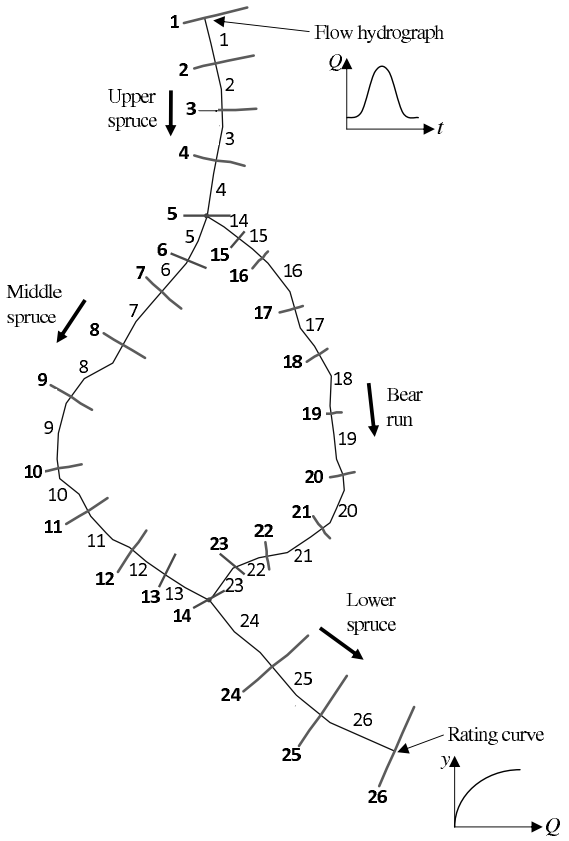

Figure 3.2: Schematic of a river system used in numerical experiments

The predictions that we use are presented in Figure 3.3. We assume 10 ensembles (or predictions) of the stream inflow. This is meant to reflect the fact that in practice several competing forecasts are used to generate different scenarios.

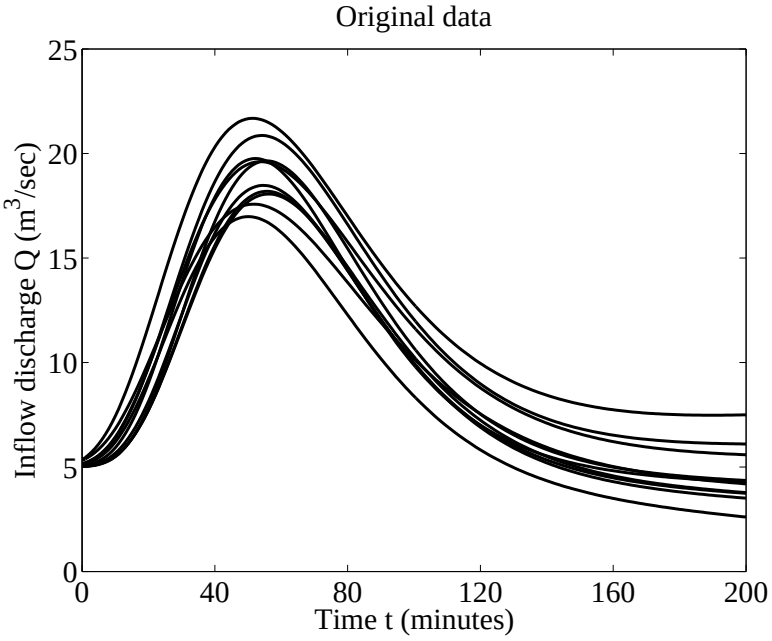

Figure 3.3: Original data

We calculate the statistical mean and covariance of the data using equations (3.5). To find a spectral representation of the covariance function of the logarithm of the stream inflow based on its eigenvalues and eigenfunctions we solve the integral equation (3.7). The first five eigenvalues are presented in the Figure 3.4. It is clear that only the first three eigenvalues are significant in terms of their magnitude: $\lambda_1 = 5.4721$, $\lambda_2 = 0.2658$, and $\lambda_3 = 0.0561$. In the Figure 3.5 we present only the eigenfunctions corresponding to the three largest eigenvalues.

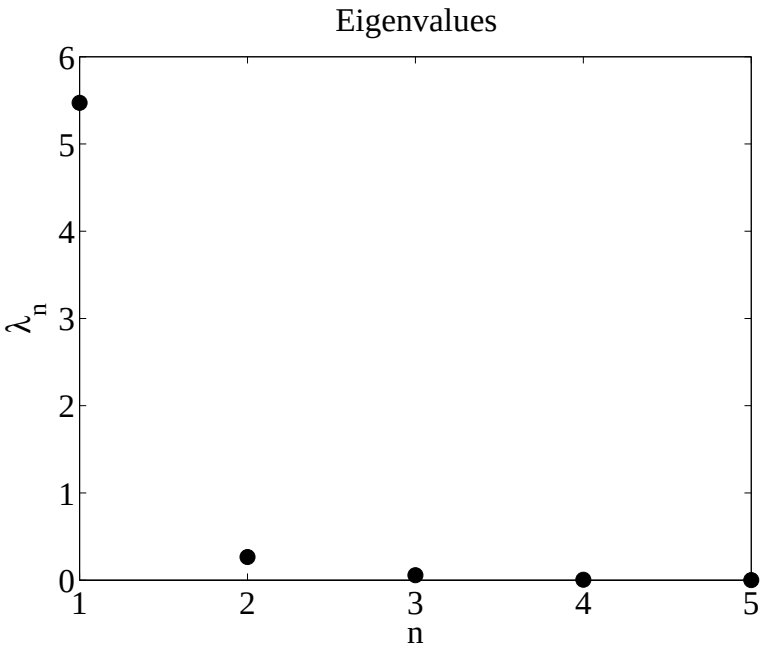

Figure 3.4: The five largest eigenvalues obtained as part of the spectral representation of the data

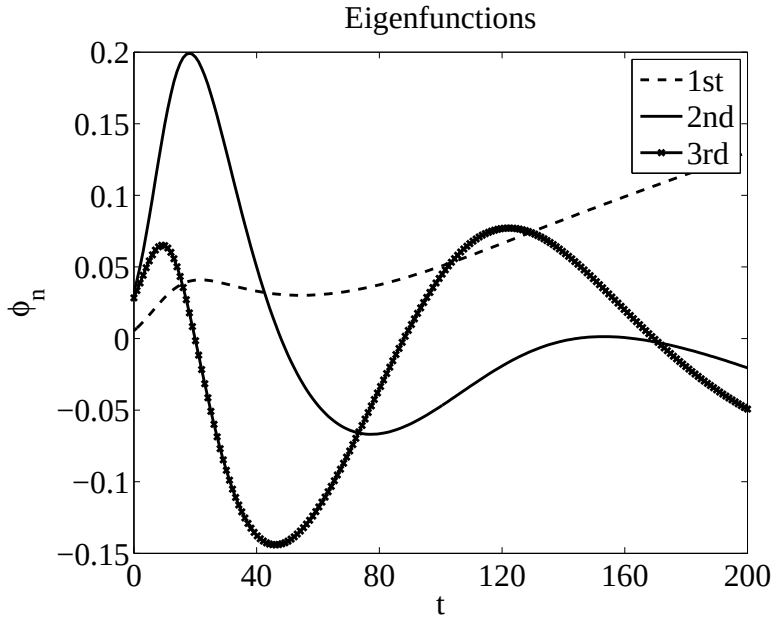

Figure 3.5: The first three eigenfunctions obtained as part of the spectral representation of the data

Since only the first 3 eigenvalues are significant we use those to produce a truncated KL representation (3.10) of the logarithm of the stream inflow function $Q_{u_1}(t)$. We use the Stochastic Collocation method to approximate the first two statistical moments of the outflow $Q_{d_{25}}$. For this demonstration, we employ 1-dimensional Gaussian quadrature points to form a full tensor grid 5×3, 5 nodes in each of the three random dimensions, although in practice a sparse grid would be used. In Figure 3.6 we present the realizations of outflow $Q_{d_{25}}$ evaluated at $5^3 = 125$ collocation points. We observe that they form five groups (and every group has five branches and twenty-five sub-branches arising due to the choice of the full tensor grid). The mean outflow, along with the mean plus and minus the standard deviation, is depicted in Figure 3.7. The deviation is the largest right after the peak due to both uncertainty in the size of the peak and its timing.

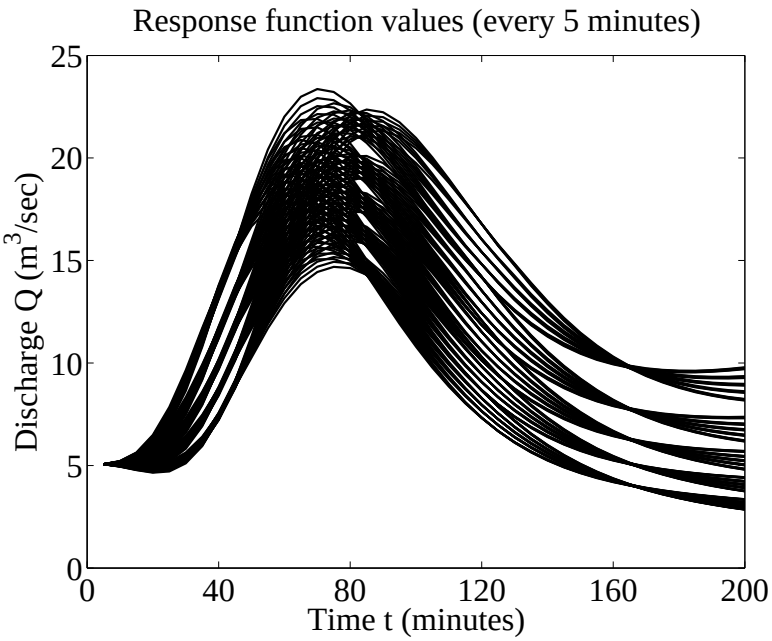

Figure 3.6: The outflow function values evaluated with the interval of 5 minutes

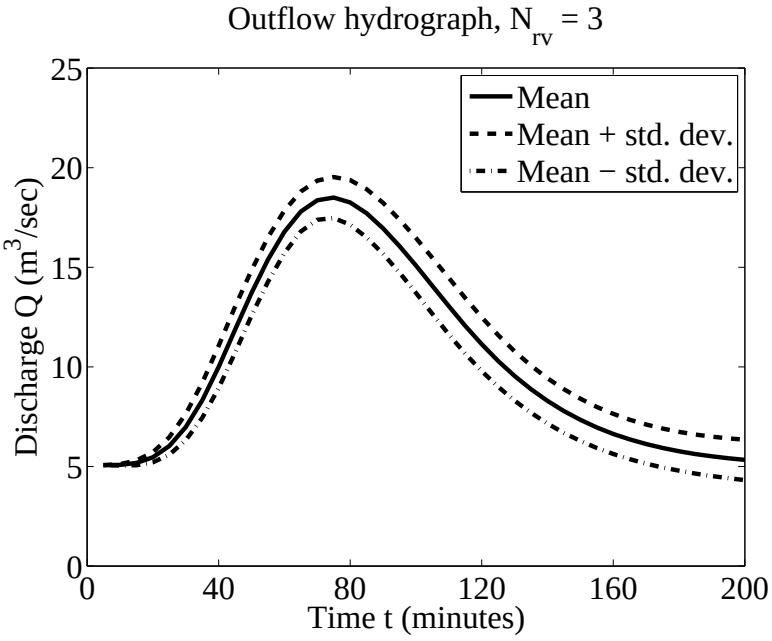

Figure 3.7: Mean plus/minus standard deviation of the response function values

The magnitude of the eigenvalues shows the contribution of the corresponding term of the Karhunen-Loève expansion to the stream inflow. In other words it explains how much of the variation in data can be expressed with the particular term. The notion of the distributional sensitivity discussed earlier in this paper shows the contribution of each term to the outflow function. We measure the sensitivity (the effect of change of the distribution on the outflow) by perturbing the distribution of the random coefficients $\{\xi_k\}_{k=1}^3$ one at a time. For the perturbed version of the density ρ_1 we use the density ρ_2 corresponding to the normal distribution with mean δ and variance $1+\varepsilon$. Table 3.1 shows the distributional sensitivity of the mean and variance of the outflow $Q_{d_{25}}$ due to the change of the mean and variance of each of the first three random variables.

We observe that the variance of the solution $Q_{d_{25}}$ is not affected if only the means of the random variables are changed. Likewise, the mean of the solution is only slightly sensitive to the variance of the random variables. We also note that the sensitivity of the mean is well-approximated by perturbing both mean and variance simultaneously (the values are the same in both cases), but the sensitivity for the variance can be off by an

Table 3.1: Distributional sensitivity of expected outflow and its variance

ξ_i	δ	ϵ	$\mathrm{DS}_{E[Q_{d_{25}}]}[\rho_1, \rho_2](Q_{d_{25}})$	$\mathrm{DS}_{\mathrm{Var}[Q_{d_{25}}]}[\rho_1, \rho_2](Q_{d_{25}})$
ξ_1	0.1	0	4.281	0.381
ξ_2	0.1	0	1.174	0.058
ξ_3	0.1	0	0.047	0.001
ξ_1	0	0.01	6.085e-3	2.069
ξ_2	0	0.01	7.952e-4	0.355
ξ_3	0	0.01	9.331e-7	0.0006
ξ_1	0.1	0.01	4.176	0.039
ξ_2	0.1	0.01	1.193	0.181
ξ_3	0.1	0.01	0.047	0.0006

order of magnitude. Additionally we observe that the magnitude of the sensitivity estimates is consistent with the arrangement of the eigenvalues in this example. The larger the eigenvalue corresponding to the particular random variable, the greater the value of the distributional sensitivity of the solution. We believe this is due to weak nonlinear dependence of the solution on the inflow function. In the case of strong nonlinearity, it is possible that the arrangement of eigenvalues would not be well correlated to the distributional sensitivities.

3.9 Conclusions and Future Work

The work presented in this paper greatly extends the applicability of the research presented in (Leon et al., 2012). We have used a Karhunen-Loève representation of a space of random inflow functions implied by a given set of ensemble predictions. We also include the distributional sensitivity estimates to help quantify the importance of each random variable in the expansion of the inflow. This approach allows fewer collocation points to be used in a particular random dimension.

Future work includes introducing inflow uncertainty into the full optimization framework, i.e., an optimal control of the dams on the multi-reservoir river network. Clearly, even a deterministic optimization problem of this complexity would require many forward simulations. With uncertainty included in the system, the computational effort increases dramatically. The uncertainty framework described in this work, together with a performance graph approach to unsteady flow routing, and fine-grained parallelism

allows to reduce the computational expenses to practical levels.

A more complete introduction of uncertainty involves the stochastic representation of the price of electricity, load and wind power generation. Each of these sources of uncertainty have different structures and require additional theory to be developed.

Acknowledgments

This research was supported in part by the Bonneville Power Administration through the Technology Innovation Program, grant number TIP-258.

Chapter 4: Conclusion

The uncertainty propagation framework and unsteady flow routing presented in this thesis are both computationally efficient and robust. In Chapter 2 it was shown that the performance graph (PG) approach can be expanded to utilize two-dimensional hydrodynamic simulations in the construction of PGs. In Chapter 3, a novel uncertainty propagation framework was detailed that utilizes Polynomial Chaos Expansion theory to propagate uncertainty in river systems. The key findings are as follows:

1. 1D-, or 2D-Computational Fluid Dynamics (CFD) programs can be used to generate PGs. Recent advancements in computer hardware and parallel programming enables batch simulations of complex CFD simulations.

2. When the river flow stays within the main-channel, the results of 1D-PGs and 2D-PGs will produce similar results. If flow exceeds the bank and enters the flood-plain however, 2D-PGs may be required.

3. Results show good agreement between flood-wave hydraulic routing between the OSU-Rivers unsteady routing model and the Telemac-2D hydrodynamics model, for a small fraction of the computational simulation time.

4. The proposed uncertainty framework is capable of propagating uncertainty through a river system, correlating system response metrics with stochastic inflows, utilizing the river dynamics. Stochastic inflows are discretized using a Karhunen-Loève expansion of the random space, and unsteady flow routing is achieved using OSU-Rivers unsteady routing model.

5. Overall, the proposed uncertainty propagation framework is numerically efficient and robust. It can be applied to any complex river system for short time-frame uncertainty propagation.

Bibliography

Abbott, M. B. (1979). Computational hydraulics: Elements of the theory of free surface flows. *Pitman, London*.

Babuška, I., Liu, K.-M., and Tempone, R. (2003). Solving stochastic partial differential equations based on the experimental data. *Math. Models Methods Appl. Sci.*, 13(3):415–444. Dedicated to Jim Douglas, Jr. on the occasion of his 75th birthday.

Babuška, I., Nobile, F., and Tempone, R. (2007). A stochastic collocation method for elliptic partial differential equations with random input data. *SIAM J. Numer. Anal.*, 45(3):1005–1034.

Bakhmeteff, B. (1932). *Hydraulics of Open Channels*. McGraw-Hill.

Celik, I. B., Ghia, U., Roache, P. J., et al. (2008). Procedure for estimation and reporting of uncertainty due to discretization in cfd applications. *Journal of Fluids Engineering*, 130(7).

Chaudhry, M. H. (2008). *Open-channel flow*. Springer, 2nd edition.

Chen, Q., Gottlieb, D., and Hesthaven, J. (2005). Uncertainty analysis for the steady-state flows in a dual throat nozzle. *J. Comput. Phys.*, 204(1):378–398.

Constantine, P. G., Doostan, A., and Iaccarino, G. (2009). A hybrid collocation/Galerkin scheme for convective heat transfer problems with stochastic boundary conditions. *Internat. J. Numer. Methods Engrg.*, 80(6-7):868–880.

Cunge, J. A., Holly, F. M., Verwey, A., et al. (1980). *Practical aspects of computational river hydraulics*, volume 3.

Fleten, S.-E. and Kristoffersen, T. K. (2008). Short-term hydropower production planning by stochastic programming. *Computers & Operations Research*, 35(8):2656–2671.

Galland, J., Goutal, N., and Hervouet, J.-M. (1991). TELEMAC: A new numerical model for solving shallow water equations. Advances in Water Resources, 14(3):138–148.

Ghanem, R. G. and Doostan, A. (2006). On the construction and analysis of stochastic models: characterization and propagation of the errors associated with limited data. *J. Comput. Phys.*, 217(1):63–81.

Ghanem, R. G., Masri, S. F., Pellissetti, M. F., and Wolfe, R. (2005). Identification and prediction of stochastic dynamical systems in a polynomial chaos basis. *Comput. Methods Appl. Mech. Engrg.*, 194(12):1641–1654.

Ghanem, R. G. and Spanos, P. D. (1991). *Stochastic finite elements: a spectral approach*. Springer-Verlag, New York.

González, J. A. and Yen, B. C. (1996). Hydraulic performance of open channel breaching. In *North American Water and Environment Congress & Destructive Water*, pages 334–339. ASCE.

González-Castro, J. A. (2000). *Applicability of the hydraulic performance graph for unsteady flow routing*. PhD thesis, Univ. of Illinois at Urbana-Champaign, Illinois.

González-Castro, J. A. and Yen, B. C. (2000). Open- channel capacity determination using hydraulic performance graph. J. Hydraul. Eng., 126(2):112–122.

Gunzburger, M. D., Peterson, J. S., and Kwon, H. (1999). An optimization based domain decomposition method for partial differential equations. *Comput. Math. Appl.*, 37(10):77–93.

Hardy, R., Lane, S., Ferguson, R., and Parsons, D. (2003). Assessing the credibility of a series of computational fluid dynamic simulations of open channel flow. *Hydrological processes*, 17(8):1539–1560.

Henderson, F. (1966). *Open channel flow*. Macmillan series in civil engineering. Macmillan.

Hervouet, J.-M. (2007). *Hydrodynamics of free surface flows : modelling with the finite element method*. John Wiley and Sons, Ltd.

Hou, T. Y., Luo, W., Rozovskii, B., and Zhou, H.-M. (2006). Wiener chaos expansions and numerical solutions of randomly forced equations of fluid mechanics. *J. Comput. Phys.*, 216(2):687–706.

Hoy, M. A. and Schmidt, A. R. (2006a). Unsteady flow routing in sewers using hydraulic and volumetric performance graphs. Proc. World Environmental and Water Resources Congress, Nebraska:1–10.

Hoy, M. A. and Schmidt, A. R. (2006b). Unsteady flow routing in sewers using hydraulic and volumetric performance graphs. In *World Environmental and Water Resource Congress 2006: Examining the Confluence of Environmental and Water Concerns*. ASCE.

Kleinstreuer, C. (1997). *Engineering fluid dynamics: an interdisciplinary systems approach*. Cambridge Univ. Press.

Knio, O. M. and Le Maître, O. P. (2006). Uncertainty propagation in CFD using polynomial chaos decomposition. *Fluid Dynam. Res.*, 38(9):616–640.

Labadie, J. W. (2004). Optimal operation of multireservoir systems: State-of-the-art review. *Journal of Water Resources Planning and Management*, 130(2):93–111.

Launder, B. E. and Spalding, D. (1974). The numerical computation of turbulent flows. *Computer methods in applied mechanics and engineering*, 3(2):269–289.

Leon, A., Kanashiro, E., and Gonzlez-Castro, J. (2013a). Fast approach for unsteady flow routing in complex river networks based on performance graphs. *Journal of Hydraulic Engineering*, 139(3):284–295.

Leon, A. S., Gibson, N. L., and Gifford-Miears, C. (2012). Toward reduction of uncertainty in complex multi-reservoir river systems. In *The XIX International Conference on Computational Methods in Water Resources*. University of Illinois at Urbana-Champaign.

Leon, A. S., Kanashiro, E. A., Valverde, R., and Sridhar, V. (2013b). A dynamic framework for intelligent control of river flooding-a case study. *Journal of Water Resources Planning and Management*.

Mahmood, K., Yevjevich, V. M., and Miller, W. A. (1975). *Unsteady flow in open channels*, volume 1. Water Resources Publications Fort Collins, Colorado, USA.

Marzouk, Y. and Xiu, D. (2009). A stochastic collocation approach to Bayesian inference in inverse problems. *Commun. Comput. Phys.*, 6(4):826–847.

Mathelin, L., Hussaini, M. Y., and Zang, T. A. (2005). Stochastic approaches to uncertainty quantification in CFD simulations. *Numer. Algorithms*, 38(1-3):209–236.

Narayan, A. and Xiu, D. (2011). Distributional sensitivity for uncertainty quantification. *Commun. Comput. Phys.*, 10(1):140–160.

Payne, J. T., Wood, A. W., Hamlet, A. F., Palmer, R. N., and Lettenmaier, D. P. (2004). Mitigating the effects of climate change on the water resources of the columbia river basin. *Climatic Change*, 62(1-3):233–256.

Ponce, V. M., Simons, D. B., and Li, R.-M. (1978). Applicability of kinematic and diffusion models. *Journal of the Hydraulics Division*, 104(3):353–360.

Rastogi, A. K. and Rodi, W. (1978). Predictions of heat and mass transfer in open channels. *Journal of the Hydraulics Division*, 104(3):397–420.

Rodi, W. (1993). *Turbulence Models and Their Application in Hydraulics, A state-of-the-art review*. A.A. Balkema, Rotterdam, third edition.

Schmidt, A. R. (2002). *Analysis of stage-discharge relations for open-channel flows and their associated uncertainties*. PhD thesis, University of Illinois at Urbana-Champaign.

Tsai, C. W. (2003). Applicability of kinematic, noninertia, and quasi-steady dynamic wave models to unsteady flow routing. *Journal of Hydraulic Engineering*, 129(8):613–627.

Versteeg, H. K. (2007). *An introduction to computational fluid dynamics the finite volume method*. Pearson Education India, 2nd edition.

Xiu, D. (2010). *Numerical Methods for Stochastic Computations. A Spectral Method Approach*. Princeton University Press, Princeton, NJ.

Xiu, D. and Hesthaven, J. S. (2005). High-order collocation methods for differential equations with random inputs. *SIAM J. Sci. Comput.*, 27(3):1118–1139.

Xiu, D. and Karniadakis, G. E. (2002). The Wiener-Askey polynomial chaos for stochastic differential equations. *SIAM J. Sci. Comput.*, 24(2):619–644 (electronic).

Xiu, D. and Sherwin, S. J. (2007). Parametric uncertainty analysis of pulse wave propagation in a model of a human arterial network. *J. Comput. Phys.*, 226(2):1385–1407.

Yen, B. C. and González-Castro, J. A. (2000). "Open- channel capacity determination using hydraulic performance graph". J. Hydraul. Eng., 126(2):112–122.

Zimmer, A., Schmidt, A., Ostfeld, A., and Minsker, B. (2013). New method for the offline solution of pressurized and supercritical flows. *Journal of Hydraulic Engineering*, 139(9):935–948.

APPENDICES

Appendix A: Fraser River Hydraulic Performance Graphs

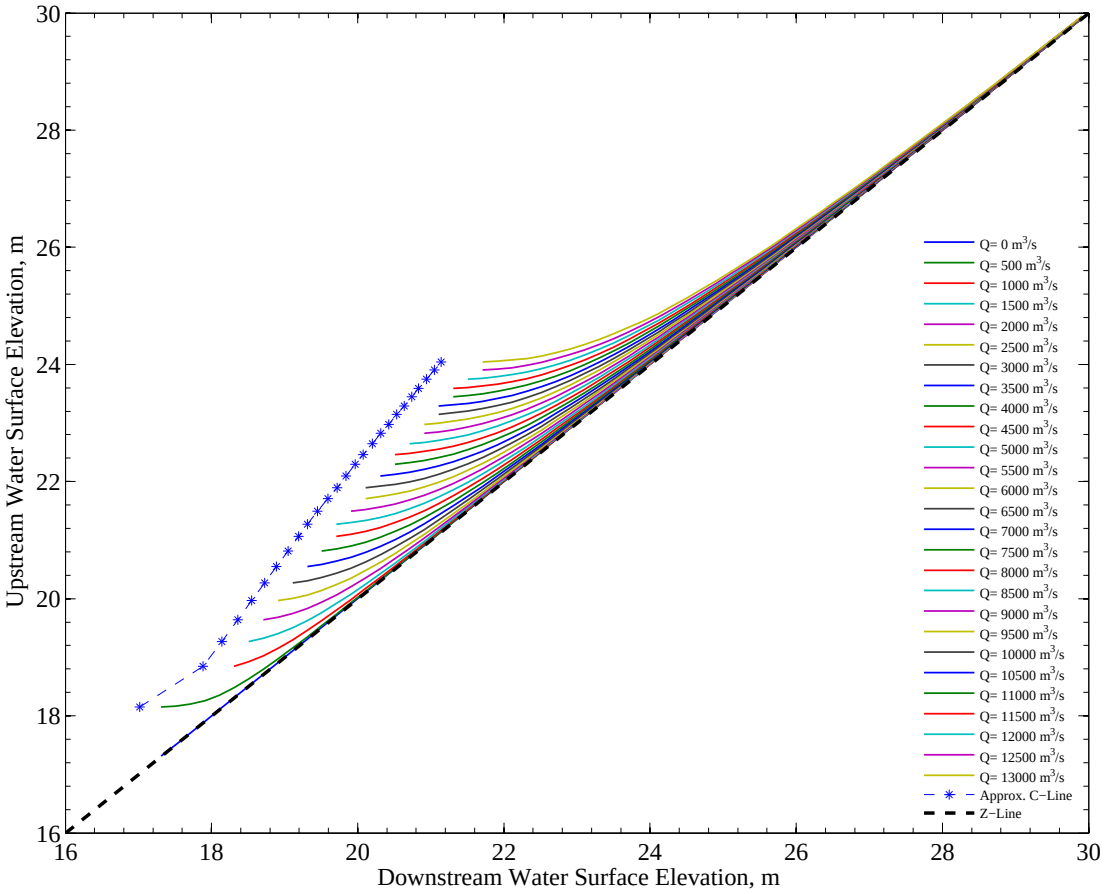

Figure A.1: Hydraulic Performance Graph generated using Telemac-2D

Appendix B: Fraser River Volumetric Performance Graphs

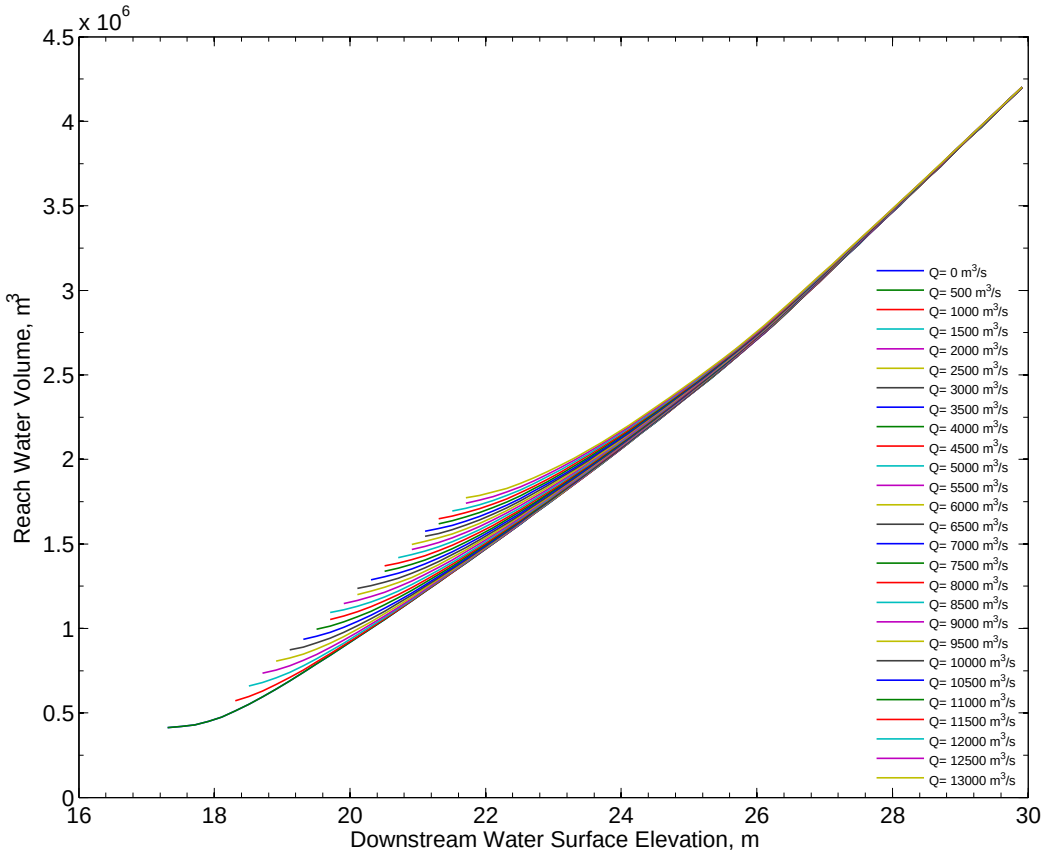

Figure B.1: Volumetric Performance Graph generated using Telemac-2D

Appendix C: Parallel batch script code

```
::=================================================================
:: TELEMAC2D_BATCH_FILE( /0 , maxProc, hpg_id )
::=================================================================
:: TELEMAC-2D Performance Graph Batch File
:: Date created:  09/16/13
:: Date modified: 09/16/13

:: Modified By: Chris Gifford-Miears
:: Purpose: run the telemac2d simulations in an "embarrassingly parallel"
:: fashion starting an independent simulation on each respective thread.
:: modified from:
:: http://stackoverflow.com/questions/672719/parallel-execution-of-shell-processes
:: example of running on DOS prompt:
:: 1. >cd *batch_file_directory
:: 2. batch_file_directory>TELEMAC2D_BATCH_FILE /O 4 HPG-4

@echo off
setlocal enableDelayedExpansion
TITLE "T2D BATCH SIMULATION - %3"
:: Display the output of each process if the /O option is used
:: else ignore the output of each process
if /i "%~1" equ "/O" (
  set "lockHandle=1"
  set "showOutput=1"
) else (
  set "lockHandle=1^>nul 9"
  set "showOutput="
)
::---------------------------------------------------------------------------
:: List of commands goes here. Each command is prefixed with :::
::: telemac2d.py
C:\0_GiffordMiears\SVNs\00_2D_HPG_checkout\hpg_3_cas_files\t2d_input\fraser_hpg_3_0_1.cas
::: telemac2d.py
C:\0_GiffordMiears\SVNs\00_2D_HPG_checkout\hpg_3_cas_files\t2d_input\fraser_hpg_3_0_2.cas
::: telemac2d.py
C:\0_GiffordMiears\SVNs\00_2D_HPG_checkout\hpg_3_cas_files\t2d_input\fraser_hpg_3_0_63.cas
::: telemac2d.py
C:\0_GiffordMiears\SVNs\00_2D_HPG_checkout\hpg_3_cas_files\t2d_input\fraser_hpg_3_0_64.cas
::---------------------------------------------------------------------------
:: Define the maximum number of parallel processes to run.
:: Each process number can optionally be assigned to a particular server
:: and/or cpu via psexec specs (untested).
set "maxProc=%2"

:: Optional - Define CPU targets in terms of PSEXEC specs
::           (everything but the command)
::
:: If a cpu is not defined for a proc, then it will be run on the local machine.
:: I haven't tested this feature, but it seems like it should work.
::
:: set cpu1=psexec \\server1 ...
:: set cpu2=psexec \\server1 ...
:: set cpu3=psexec \\server2 ...
```

```
:: etc.

:: For this demo force all cpu specs to undefined (local machine)
for /l %%N in (1 1 %maxProc%) do set "cpu%%N="

:: Get a unique base lock name for this particular instantiation.
:: Incorporate a timestamp from WMIC if possible, but don't fail if
:: WMIC not available. Also incorporate a random number.
  set "lock="
  for /f "skip=1 delims=-+ " %%T in ('2^>nul wmic os get localdatetime') do (
    set "lock=%%T"
    goto :break
  )
  :break
  set "lock=%temp%\lock%lock%_%random%_"

:: Initialize the counters
  set /a "startCount=0, endCount=0"

:: Clear any existing end flags
  for /l %%N in (1 1 %maxProc%) do set "endProc%%N="

:: Launch the commands in a loop
  set launch=1
  for /f "tokens=* delims=:" %%A in ('findstr /b ":::" "%~f0"') do (
    if !startCount! lss %maxProc% (
      set /a "startCount+=1, nextProc=startCount"
    ) else (
      call :wait
    )
    set cmd!nextProc!=%%A
    if defined showOutput echo
    ------------------------------------------------------------------------------
    echo !time! - proc!nextProc!: starting %%A
    2>nul del %lock%!nextProc!
    %= Redirect the lock handle to the lock file. The CMD process will     =%
    %= maintain an exclusive lock on the lock file until the process ends. =%
    start /b "" cmd /c %lockHandle%^>"%lock%!nextProc!" 2^>^&1 !cpu%%N! %%A
  )
  set "launch="

:wait
:: Wait for procs to finish in a loop
:: If still launching then return as soon as a proc ends
:: else wait for all procs to finish
  :: redirect stderr to null to suppress any error message if redirection
  :: within the loop fails.
  for /l %%N in (1 1 %startCount%) do (
    %= Redirect an unused file handle to the lock file. If the process is    =%
    %= still running then redirection will fail and the IF body will not run =%
    if not defined endProc%%N if exist "%lock%%%N" (
      %= Made it inside the IF body so the process must have finished =%
      if defined showOutput echo
```

```
      ================================================================================
      echo !time! - proc%%N: finished !cmd%%N!
      if defined showOutput type "%lock%%%N"
      if defined launch (
        set nextProc=%%N
        exit /b
      )
      set /a "endCount+=1, endProc%%N=1"
    ) 9>>"%lock%%%N"
  ) 2>nul
  if %endCount% lss %startCount% (
    1>nul 2>nul ping /n 2 ::1
    goto :wait
  )

2>nul del %lock%*
if defined showOutput echo
================================================================================
echo ============================================================
echo Cheers^^!
echo CGM
echo ============================================================
EXIT /bSUB
```